Ore Geology Reviews 182 (2025) 106660

Contents lists available at ScienceDirect

Ore Geology Reviews

journal homepage: www.elsevier.com/locate/oregeorev

# Evidence for metal sources, fluid-mixing processes, and S isotope recycling within the feeder zone of an Irish type Zn-Pb deposit

Aileen L. Doran [a,b,*], Steven P. Hollis [c], Julian F. Menuge [b], Connor Lyons [b,d], Stephen J. Piercey [e], Adrian J. Boyce [f], Paul Slezak [g], Koen Torremans [b], John Güven [b]

[a] Satarla, 2nd Floor, 52 Horseferry Road, Westminster, London SW1P 2AF, UK
[b] SFI Research Centre in Applied Geosciences (iCRAG), School of Earth Sciences, University College Dublin, Belfield, Dublin 4, Ireland
[c] School of GeoSciences, Grant Institute, King's Buildings, The University of Edinburgh, Edinburgh EH9 3JW, UK
[d] 175-503 East Broadway, Vancouver, BC V5T 1W2, Canada
[e] Department of Earth Sciences, Memorial University of Newfoundland, 300 Prince Philip Drive, St. John's, Newfoundland A1B 3X5, Canada
[f] Scottish Universities Environmental Research Centre (SUERC), Rankine Avenue, East Kilbride, Glasgow G75 0QF, UK
[g] Idaho National Lab, Center for Advanced Energy Studies, 995 MK Simpson Blvd, Idaho Falls, ID 83401, USA

ARTICLE INFO

*Keywords:*
Irish-type deposits
$\delta^{34}S$ isotopes
Sulphide replacement
Hydrothermal Ni
Sulphide mineral chemistry

ABSTRACT

The origin and evolution of fluids in Irish-type Zn-Pb deposits remains debated, particularly regarding the mobility of metals such as Cu and Ni, sources of sulphur, and the role of fluid mixing and replacement. The Lisheen Zn-Pb deposit, Ireland, offers a well-defined natural laboratory to investigate these questions. While most studies have focused on the Waulsortian Limestone Formation, the primary sulphide host, less is known about mineralisation in underlying units, such as the Lisduff Oolite Member (LOM). The LOM displays enrichment in Cu and Ni and displays intense replacement textures compared to other hosts at Lisheen, making it an ideal target for studying metal mobility and sulphur recycling in carbonate-hosted systems. Through characterising and studying LOM-hosted sulphides, valuable insights into mineralisation processes, especially related to Cu-Ni metals, can be defined. This study integrates petrography, EMPA, and in situ sulphur isotope ($\delta^{34}S$) analysis to investigate sulphide paragenesis, mineral chemistry, and fluid evolution across LOM ore zones. Results reveal a multistage mineralising system involving extensive replacement of early pyrite (Py0, $\delta^{34}S = -28.4$ to $-21.9$ ‰) by sphalerite and galena, with zoned pyrite (Py1) enriched in As-Cu-Ni-Tl. The $\delta^{34}S$ values and trace element trends indicate mixing between hydrothermal and bacteriogenic sulphur-rich fluids, with evidence for sulphur recycling during replacement. Pyrite textures and compositions capture this evolving fluid regime, with trace element enrichment linked to paragenetic stage. The steel ore region, adjacent to major fault intersections, records intense hydrothermal fluid interaction, hosting Ni- and As-rich phases such as nickeline, gersdorffite, and arsenopyrite. These findings highlight the importance of structural controls and fluid mixing in metal transport and deposition, positioning the LOM as a key stratigraphic unit for understanding ore-forming processes in Irish-type systems. These results have implications for targeting similar carbonate-hosted systems globally, especially where deeper or structurally complex ore zones remain underexplored.

## 1. Introduction

Sediment-hosted Zn-Pb deposits are important global source of metals, with the two main deposit types, sedimentary exhalative (SEDEX) and Mississippi Valley-type (MVT), hosting ~50 % of the world resources of Zn and Pb (Wilkinson, 2014). Since the 1960s, Ireland has been an important contributor of Zn and Pb in Europe (Ashton et al., 202). Irish-type deposits are a type of structurally controlled, carbonate-hosted mineralisation, with characteristics considered to be transitional between both MVT and SEDEX deposits (Wilkinson, 2014). Currently only the Navan Zn-Pb mine remains operational, but Ireland has a long history of exploration and mining, with past deposits (e.g. Lisheen, Galmoy) facilitating important social and economic growth across Ireland (AECOM, 2020). These deposits are not unique to Ireland, however, with several global occurrences sharing similar geological, mineralogical and genetic features. Examples include Gays River (Nova

* Corresponding author at: Satarla, 2nd Floor, 52 Horseferry Road, Westminster, London SW1P 2AF, UK.
*E-mail address:* aileen.doran@satarla.com (A.L. Doran).

https://doi.org/10.1016/j.oregeorev.2025.106660
Received 2 February 2024; Received in revised form 18 April 2025; Accepted 4 May 2025
Available online 8 May 2025

Scotia), of similar host rock and mineralization ages to the Irish deposits, and which displays overlapping fluid and sulphide precipitation mechanisms (e.g., temperature, fluid mixing) to Irish Zn-Pb systems (Savard and Chi, 1998; Wilkinson, 2014). The Prairie Creek sulphides of the Northwest Territories, Canada, have also been compared to Irish-type due to their similar mineralogy, carbonate-replacement associations, and structural and stratabound control on fluid migration and mineralisation (Paradis, 2007; Wilkinson, 2014). Similarly, the Reocín deposit of Spain is hosted in dolomitised carbonate, with stratabound and structurally-controlled mineralisation, comparable to Irish-type (Velasco et al., 2003; Wilkinson, 2014). Iranian Zn-Pb deposits are associated with an extensional regime related to back-arc spreading and formation in Early Cretaceous carbonate sediments are considered Irish-type (Rajabi et al. 2023). The Sedmochislenitsi Zn-Pb-Cu-Ag deposit, NW Bulgaria, also displays similarities to Irish-type, with mineralisation found adjacent to possible feeder faults (Andrew, 2023).

In the southern Irish orefield, Zn-Pb mineralisation is interpreted to have formed through replacement of hydrothermally altered Lower Carboniferous/Mississippian limestones (Hitzman and Large, 1996; Blakeman et al., 2002; Hitzman et al., 2002; Fusciardi et al., 2003; Wilkinson et al., 2005). Dissolution-precipitation reactions and replacement and open space/fracture infill were the key processes responsible for ore deposition (Hitzman and Large, 1996; Wilkinson et al., 2005). The generation of significant sulphide mineralisation was contingent on the presence of an extensive fault network, with Waulsortian Limestone Formation-hosted deposits typically found in normal fault zones (Boyce et al., 1983a; Hitzman and Large, 1986; Hitzman et al., 1992; Johnston et al., 1996; Hitzman, 1999; Hitzman et al., 2002; Fusciardi et al., 2003; Torremans et al., 2018; Kyne et al., 2019). These faults acted as feeder conduits for ascending, hot (up to 280 ℃), metal-bearing hydrothermal fluids containing limited sulphur, that then mixed with descending, cooler (<100 ℃) hypersaline brines carrying bacteriogenically reduced sulphur to form the ore bodies (Boyce et al., 1983b; Hitzman and Large, 1986; Anderson et al., 1998; Everett et al., 1999; Hitzman, 1999; Fallick et al., 2001; Banks et al., 2002; Blakeman et al., 2002; Wilkinson et al., 2005; Wilkinson et al., 2009; Wilkinson, 2010).

Irish-type Zn-Pb deposits have generally been well studied, with research primarily focusing on Waulsortian Limestone Formation-hosted Zn-Pb mineralisation, with limited work on the paragenesis and geochemistry of other stratigraphic hosts, such as the underlying Lisduff Oolite Member (LOM) which can be associated with Cu and Ni enrichments. As a result, these other mineralised stratigraphic units within a system can provide crucial insights into fluid sources and

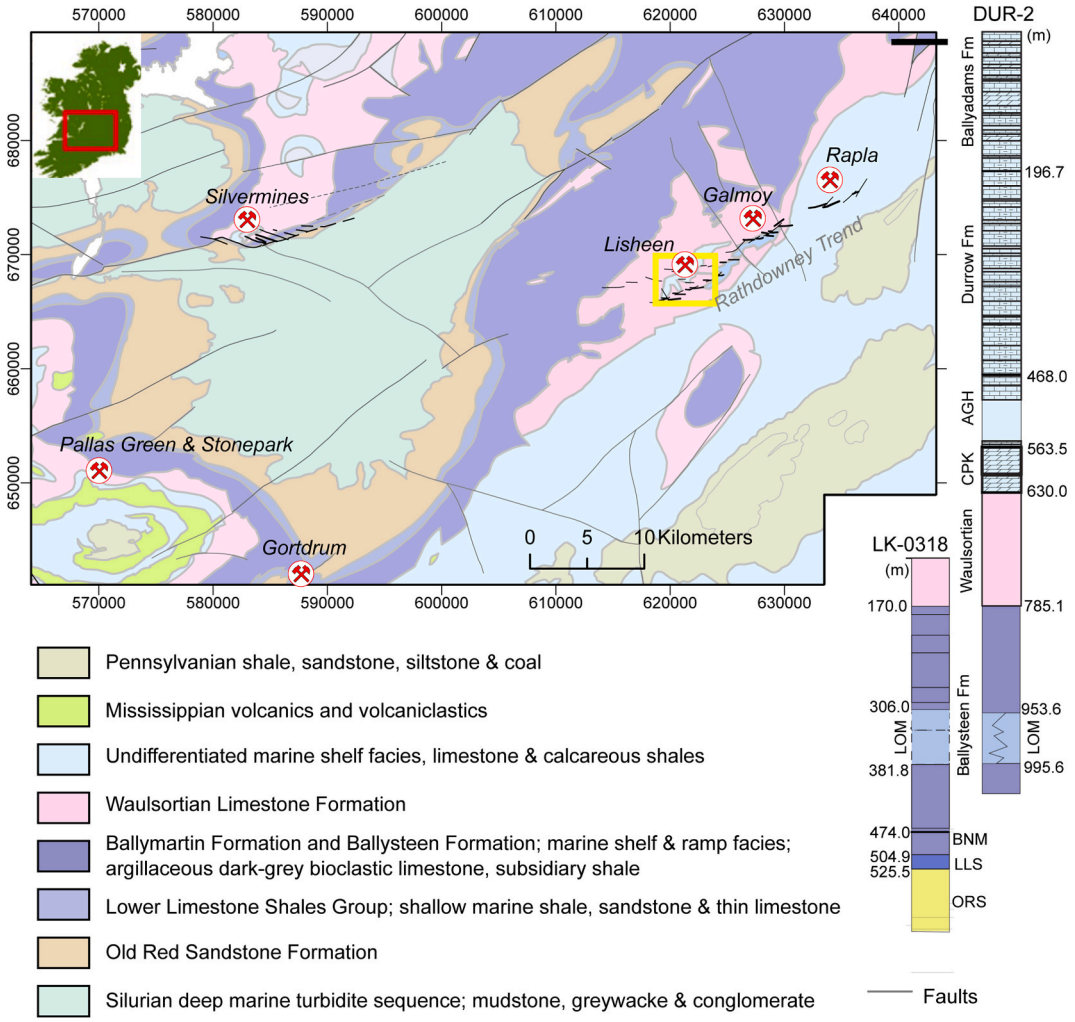


**Fig. 1.** Geological map of the southern Irish Zn-Pb Orefield regional geology, showing location of main mineral deposits and prospects. The region referred to as the Rathdowney Trend and past mines/current prospects are highlighted, including Lisheen and Rapla. A yellow box is included to highlight the location of the Lisheen mine, as shown in Fig. 2. Geology is modified from Geological Survey Ireland (2014), incorporating observations from mapping and modelling data by authors. The lithostratigraphic columns show stratigraphy from two regional stratigraphic boreholes, LK-0318 from the Lisheen deposit and DUR-2 from Rapla. Abbreviations: LOM: Lisduff Oolite Member; AGH: Aghmacart Formation; CPK: Crosspatrick Formation; LLS: Lower Limestone Shale Group; ORS: Old Red Sandstone Formation. (For interpretation of the references to colour in this figure legend, the reader is referred to the web version of this article.)

evolution, along with the overall mineralisation processes. Copper has been seen in other Irish systems such as Gortdrum, which remains the only orebody mined in the Irish midlands primarily for Cu and has a similar structural framework to Lisheen (Cordeiro et al., 2023; Dunlevy et al., 2023). There are several other significant Cu associations in the southwest of the Irish Orefield, such as Tynagh and Kilbricken (Ashton et al., 2023), with Ni also associated with Galmoy (Güven et al., 2023). However, detailed studies on the origin and paragenetic associations of Cu-Ni are often lacking, with a lot of uncertainty around the origin and mobility pathways of both Cu and Ni in the Irish Orefield (e.g., Wilkinson, 2023).

The Lisheen deposit is situated in the southern Irish Zn-Pb orefield (Fig. 1), was the second largest mined Zn-Pb deposit in Ireland, with the resource (23 Mt @ 13.3 % Zn and 2.3 % Pb; Güven et al., 2023) mined from 1999 until 2015 (Hitzman et al., 2002; Torremans et al., 2018; Kyne et al., 2019). At Lisheen, mineralisation is predominantly hosted by the Waulsortian Limestone Formation, which has been the focus of most published research (e.g., Hitzman et al., 2002; Fusciardi et al., 2003; Wilkinson et al., 2005). However, while minor, significant resources are located in the LOM of the underlying Ballysteen Formation, with notable Cu-Ni associations (Fig. 2; e.g., Fusciardi et al. 2003; Wilkinson et al., 2005). LOM-hosted ores typically occur adjacent to significant feeder faults (Fig. 2b), have considerable host rock brecciation and sulphide replacement textures and thus allow investigation of the possibility of metal and sulphur recycling in LOM-hosted mineralisation and comparisons to Waulsortian Limestone Formation-hosted mineralisation (Doran et al., 2022). Furthermore, high concentrations of Cu and Ni observed in the LOM are unusual for Irish-type deposits and provide an opportunity to further elucidate potential sources and mobility of metals (e.g., Ni and Cu) in Ireland, and sediment-hosted hydrothermal systems more broadly.

We present the first detailed petrographic descriptions, paragenetic interpretation, *in situ* $\delta^{34}S$ isotope values and trace element geochemistry from LOM-hosted mineralisation at Lisheen, and provide a refined understanding of mineral formation and replacement processes. This research additionally highlights the importance of pyrite mineral chemistry in tracing fluid mixing processes and metal sources in Irish-type Zn-Pb deposits, and unravelling metal mobility in hydrothermal systems. The insights gained from this study can offer new understandings of fluid and ore forming processes in similar deposits globally, potentially offering new ways to guide exploration in other carbonate-hosted systems.

## 2. Geological setting

### 2.1. Regional geology

The geology of the Irish Zn-Pb orefield has been the focus of numerous past studies, with many presenting extensive reviews of the geological and structural evolution (e.g., Philcox, 1984; Hitzman et al., 2002; Kyne et al., 2019; Doyle, 2022; Güven et al., 2023). Here we present a summary of the geological and structural evolution of the southern Irish Zn-Pb orefield to constrain key understandings for the area. The southern Irish orefield is underlain by deformed Lower Palaeozoic sedimentary rocks, which in turn are unconformably overlain by Devonian to early Carboniferous terrestrial mudstones, conglomerates and sandstones comprising the Old Red Sandstone (ORS; Philcox, 1984; Wilkinson et al., 2005; Walshaw et al., 2006). Conformably overlying the ORS are Mississippian carbonates, representing a northward marine transgressive succession on a carbonate ramp evolving into a carbonate platform, accentuated locally by faults (Philcox, 1984; Andrew, 1986; Hitzman et al., 1998; Johnston, 1999; Doyle, 2022). In some areas carbonates are interbedded with minor alkaline basaltic rocks (Slezak et al., 2022), although this is not the case in the Rathdowney Trend and so is not considered further. Near the Lisheen deposit, the Mississippian stratigraphy is subdivided into the Mellon House, Ringmoylan, Ballymartin, Ballysteen, Waulsortian Limestone and Crosspatrick formations (Philcox, 1984; Hitzman et al.,

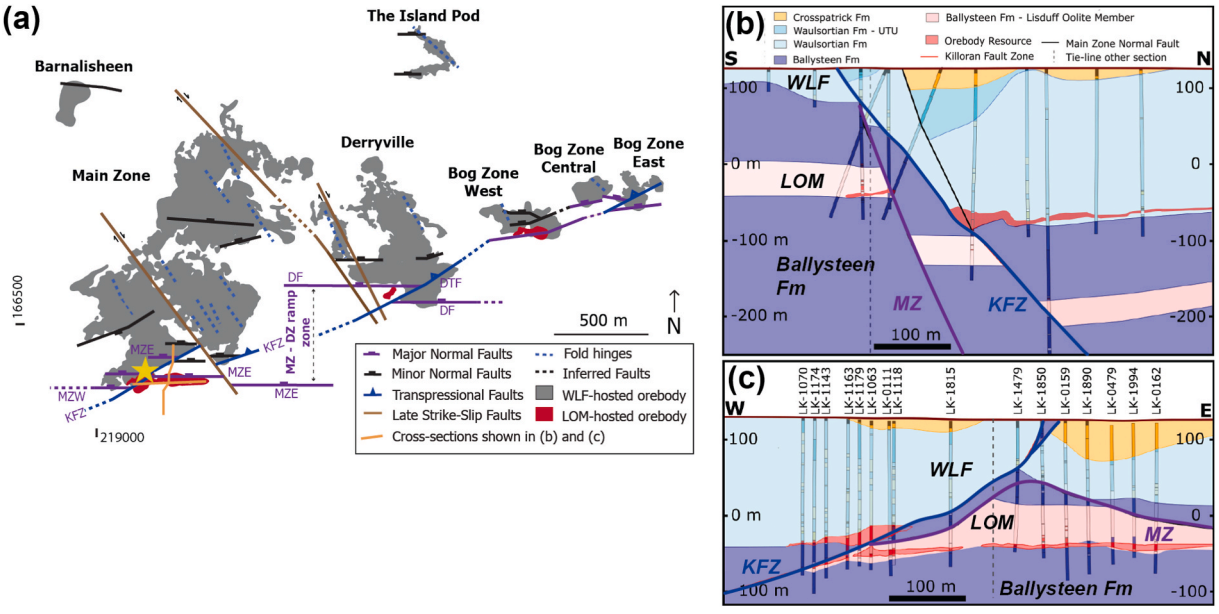


**Fig. 2.** (a) Surface projection of the Lisheen orebodies, displaying key structural features. Major normal faults are shown by purple lines. LOM-hosted mineralisation occurs in the immediate footwall north of the E-W trending Main Zone East Fault (MZE), a Mississippian normal fault that, prior to structural deformation, connected with Main Zone West (MZW) via a breached relay ramp. The MZE was later deformed by the Killoran Fault Zone (KFZ), a NE-trending Mississippian normal fault which has subsequently been reactivated by dextral oblique-reverse slip during the Variscan orogeny, displacing original HW-FW fault juxtapositions. Steel ore mineralisation occurs throughout LOM-hosted zones, often observed near faults. The location of the steel ore region included in this study is shown by the yellow stars. Other nomenclature (DF: Derryville Fault; DTF: Derryville Transpressional Fault; MZ-DZ: Main Zone – Derryville Zone). Structural features adapted from Torremans et al. (2018) and Kyne et al. (2019). For a full review of the structural evolution at Lisheen mine, please refer to Kyne et al. (2019) (b) Cross-section of the S-N orange line shown in (a), with representative drill cores used for the cross-section shown. (c) Long-section of the W-E orange line shown in (a), with drill cores used for the cross-section shown. (For interpretation of the references to colour in this figure legend, the reader is referred to the web version of this article.)

2002; Doyle, 2022). While these stratigraphic intervals are not always observed in a single log, representative stratigraphic logs are shown in Fig. 1, based on drillholes LK-0138, LK-0290 at Lisheen, and DUR-2 at Rapla for the upper stratigraphies. Sulphide mineralisation is typically hosted in the Ballysteen and Waulsortian Limestone formations (Fig. 2a), forming what is known as Irish-type Zn-Pb mineralisation.

The Irish-type Zn-Pb deposits are associated with a complex tectono-stratigraphic evolution, with mineralisation strongly influenced by pre-existing Caledonian basement structures and subsequent extensional and compressional events (Kyne et al., 2019; Güven et al., 2023; Ashton et al., 2023). However, a series of interconnected extensional basins formed during the Late Devonian to Early Carboniferous, due to N-S to NNW-SSE extension events (Johnston et al., 1996; Kyne et al., 2019). This extensional activity led to the development of E-W- to NE-SW-trending normal faults, which were controlled by the geometry of underlying basement structures (Johnston et al., 1996; Johnston, 1999; Kyne et al., 2019). Known Zn-Pb deposits generally occur in the hanging wall of these normal fault systems, which present as segmented stepping normal fault arrays within the Mississippian host rocks. One of these arrays, the Rathdowney Trend, is an ~ 40 km long trend cut by a series of ENE-trending normal faults (Fig. 1; Fig. 2a-c). It includes several notable Zn-Pb deposits such as Lisheen, Galmoy and Rapla (Fig. 1; Hitzman et al., 1992; Wilkinson et al., 2011). These Early Carboniferous basins were deformed during the Late Carboniferous (Variscan) orogeny, with N-S compression and basin inversion occurring (Kyne et al., 2019; Doyle, 2022). This inversion resulted in reverse faulting and open folding, which are closely linked with Zn-Pb mineralisation, and resulted in intensified deformation adjacent to reactivated normal faults (Johnston et al., 1996; Fusciardi et al., 2003; Kyne et al., 2019). Other features associated with this inversion include formation of transpressional faults, such as those shown in Fig. 2a. These episodes of deformation were followed by NNW-trending strike-slip faults which offset all previous structures (Kyne et al., 2019).

The segmented normal fault arrays, with left-stepping geometries, which defined he Rathdowney Trend were crucial in the development of Irish Zn-Pb deposits through controlling their location and fluid flow within these systems (Kyne et al., 2019; Güven et al., 2023). Between each of these fault segments, such as those seen in Lisheen (Fig. 2a), linking structures, like relay ramps or breaching faults, formed an important control on fluid flow localisation and subsequent development of orebody geometries (Kyne et al., 2019). In particular, the occurrence of intact and breached relay ramps was important at Lisheen, leading to the development of conduits for upwelling fluids and directing of these fluids vertically and laterally into the hanging walls of bounding fault segments (Kyne et al., 2019).

### 2.2. Lisheen deposit Zn-Pb mineralisation

The Lisheen Mine closed in late 2015 and had a final pre-mining resource of 23 Mt grading 13.3 % Zn and 2.3 % Pb (Torremans et al., 2018; Güven et al., 2023). The deposit contained six stratabound orebodies: Main Zone, Derryville, Bog East, Bog Central, Bog West and the Island Pod (Fig. 2a). Additional mineralisation has been discovered at Barnalisheen (Fig. 2a) to the northwest, and at Templetouhy and Bawnmore further east. Zinc-lead mineralisation at Lisheen is generally hosted at the mostly dolomitised base of the Waulsortian Limestone Formation (Fig. 2b-c) and is often associated with hydrothermal dolomite breccias (Philips and Sevastopulo, 1986; Lee and Wilkinson, 2002; Wilkinson, 2003; Wilkinson et al., 2005; Doran, 2021). Additional zones of mineralisation are hosted within the ~ 200 m thick Ballysteen Formation (Fig. 2b), which is composed of the Lower Calcarenite Member, the Lisduff Oolite Member and the Upper Calcarenite Member (Fusciardi et al., 2003; Wilkinson et al., 2005). Pyrite Re-Os dating at Lisheen (346.6 ± 3 Ma; Hnatyshin et al., 2015) suggests mineralisation was coincident with the growth of normal faults.

### 2.3. Lisduff Oolite Member-hosted mineralisation

The Lisduff Oolite Member (LOM) (~70–80 m) lies near the base of the Mississippian sequence in the Rathdowney Trend (Fig. 1; Fig. 2b-c) and consists of oosparite to biosparite limestones (Doyle, 2022), reflecting high energy shallow marine sedimentation (Fusciardi et al., 2003). The LOM is separated into three oolite units separated by two distinctive argillaceous units, with the main differences between oolitic units defined by grain size and proportion of skeletal material (Philcox, 2004).

While the full extent of LOM-hosted mineralisation at Lisheen is unknown, it is generally thought to be structurally controlled and is often associated with brecciation of the LOM host in the footwall of faults (Passmore, 2002; Fusciardi et al., 2003; Röhner, 2017; Torremans et al., 2018; Kyne et al., 2019; Güven et al., 2023; Fig. 2b-c). LOM-hosted mineralisation is often strongly developed where the LOM is in fault contact with the Waulsortian Limestone Formation (Shearley et al., 1996; Redmond, 1997, Sevastopulo and Redmond, 1999; Hitzman et al., 2002., Fusciardi et al., 2003; Torremans et al., 2018; Kyne et al., 2019; Güven et al., 2023; Fig. 2b-c). Further, LOM-hosted mineralisation is typically dominated by replacement of host rocks and open space infill, and is interpreted to represent the first introduction of hydrothermal fluids into the Lisheen hydrothermal system (Passmore, 2002; Fusciardi et al., 2003; Kyne et al., 2019).

Previous studies of LOM-hosted mineralisation are limited, with research typically focusing on the structural development of the deposit. Consequently, LOM-hosted mineralisation has not been studied in depth, and is often not separated by ore zone across Lisheen. Below, we summarise the available data by ore zone.

*Main Zone:* The Main Zone LOM-hosted mineralisation is the most extensively developed mineralisation compared to other LOM areas mined at Lisheen. Within the Main Zone, notable dissolution has been recorded (e.g., Güven et al., 2023) with up to 30 m of the LOM stratigraphy missing above the known mineralisation. This is thought to be structurally controlled, and resulted in breccia formation due to collapse (Güven et al., 2023). Within the LOM, especially in the immediate footwall of the Killoran Fault of the Main Zone, there is an irregular body of heterogeneous breccia known locally as the Oolite Breccia likely of hydrothermal origin (Philcox, 2004).

To the west of the Main Zone, where intersecting faults brought the LOM into contact with the Waulsortian Limestone Formation (Kyne et al., 2019), there is also a region of massive Ni mineralisation in the form of niccolite / nickeline (Güven et al., 2023).

*Steel ore, Main Zone:* Within the Main Zone, another unique area of mineralisation occurs where faults intersect. This area, hosted by the LOM, is located on the structural footwall of the Killoran fault (Fig. 2) and is defined by fine, dark massive sulphide (galena, sphalerite) zones that have a dark grey/steel lustre underground (Güven et al., 2023). This zone of dark mineralisation was locally referred to as the 'steel ore' region by Lisheen mine geologists. While volumetrically low relative to standard LOM-hosted mineralisation, the steel ore contains extensive galena and sphalerite replacement of earlier sulphides.

*Derryville Zone:* Derryville LOM-hosted mineralisation occurrences are not as extensively developed as those hosted by the Main Zone. However, while not as widely drilled, mineralisation appears to be genetically similar to Main Zone equivalents (Güven et al., 2023).

*Ramp Zone:* There is very limited data published on the oolite of the Ramp Zone between Main Zone and Derryville Zone. The Ramp Zone refers to the relay-ramp between Main and Derryville zones, and importantly acted as a fluid pathway for hydrothermal fluid migration (Kyne et al., 2019). As a result, mineralisation is minor, but represents sulphide development during the migration of hydrothermal fluids. There are similar relay-ramp zones identified between other ore zones (e.g., Derryville and Bog Zone; Kyne et al., 2019).

LOM-hosted mineralisation has high Zn-Pb tonnages, low Zn/Pb ratios and higher Cu, Ni, Co, Ag and As grades than mineralisation

elsewhere in the Lisheen deposit (Torremans et al., 2018; Fig. 3). The elevated Zn-Pb tonnages and low Zn/Pb ratios are similar to feeder-zone signatures for other Waulsortian Limestone Formation-hosted mineralisation adjacent to major normal faults (Fusciardi et al., 2003; Torremans et al., 2018). Generalised cross sections of the LOM, its associated mineralisation and metal trends, and relationships to structures are shown in Fig. 2b and 3.

## 3. Methods

Drill core and stockpile samples (100 + ) were selected for petrographic study to cover all observed sulphide and carbonate phases and to broadly represent the LOM-hosted mineralisation from the Main, Derryville and Ramp zones at Lisheen (Fig. 2a). Samples were examined using transmitted and reflected light microscopy, cathodoluminescence (CL) and scanning electron microscope (SEM). A Nikon Eclipse LV100Npol microscope and Hitachi TM3030Plus Tabletop SEM were used for petrographic investigations at University College Dublin (UCD), Ireland. Cathodoluminescence imaging was carried out using a CITL mk5 cold CL stage, mounted on a Nikon 50i microscope with a Nikon digital camera at Imperial College, London, UK.

### 3.1. Electron microprobe analyses (EMPA) of pyrite and galena

Based on the initial petrographic work, a sub-set of samples (n = 8), representing the key pyrite and galena textures was selected for mineral chemistry analysis. Analyses of pyrite (n = 421) are from across LOM-hosted mineralisation, while galena samples (n = 28) are only from the steel ore region (Fig. 2a). An overview of selected pyrite data, focusing on two specific samples, is presented in Table 1, with the full dataset included in Electronic Supplement Material (ESM) 1, along with detection limits. Data were obtained using a JEOL JXA-8230 EPMA at Memorial University in Newfoundland, Canada, with an accelerating voltage of 20 kV, a beam current of 10 nA and a spot size of 3–4 μm. Pyrite was analysed for S, Fe, As, Co, Ni, Cu, Ag, Tl and Pb; Mn, Mo, Cd, Sb, Au, and Bi are below detection limit and data are not presented here. Galena was analysed for S, Pb, Fe, As, Co, Ni, Cu, Ag, Tl, Sb, Bi, Cd, Au, Mo and Mn with data for Ag through Mn below detection limits. Detection limits for all reported elements were 0.01 wt%, excluding Zn, Ag, Tl, and Ni which had detection limits of 0.02 wt% (ESM 1). In-house standards of known composition (e.g. pyrite, arsenopyrite, galena) were measured throughout the period of analysis for quality control. Data was reduced using a ZAF matrix correction.

### 3.2. Sulphur isotope analyses

*In situ* laser combustion sulphur isotope analysis of pyrite, galena and sphalerite from 10 samples, each presented as a polished block, was undertaken at the Scottish Universities Environmental Research Centre (SUERC), UK. The sample blocks were held in a chamber filled with pure oxygen gas and a Spectron Lasers 902Q CW Nd: YAG laser (1 W power) operating in TEM00 mode was used to ablate individual minerals. Laser application onto the pre-selected minerals resulted in sulphide combustion with subsequent $SO_2$ gas generation. Laser use left behind ~ 50 μm wide ablation tracks, ensuring contamination from other phases was limited. The resulting $SO_2$ gas was purified through several heating and cooling steps along a glass extraction line, with water vapor and $CO_2$ being removed using a $CO_2$ and acetone slush trap and a n-pentane trap, respectively (following Robinson and Kusakabe, 1975). The purified $SO_2$ gas was sequestered and moved to a VG SIRA II gas mass spectrometer, to measure the $\delta^{66}SO_2$ value of each sample. The $\delta^{66}SO_2$ value was then converted to $\delta^{34}S$ values and corrected, with sample precision typically < 0.3 ‰ (1σ). Further information on this technique is given by Wagner et al. (2002). Resulting sulphur isotope data are shown using the conventional delta (δ) value notation relative to Vienna Canyon Diablo Troilite V-CDT standard (Table 2).

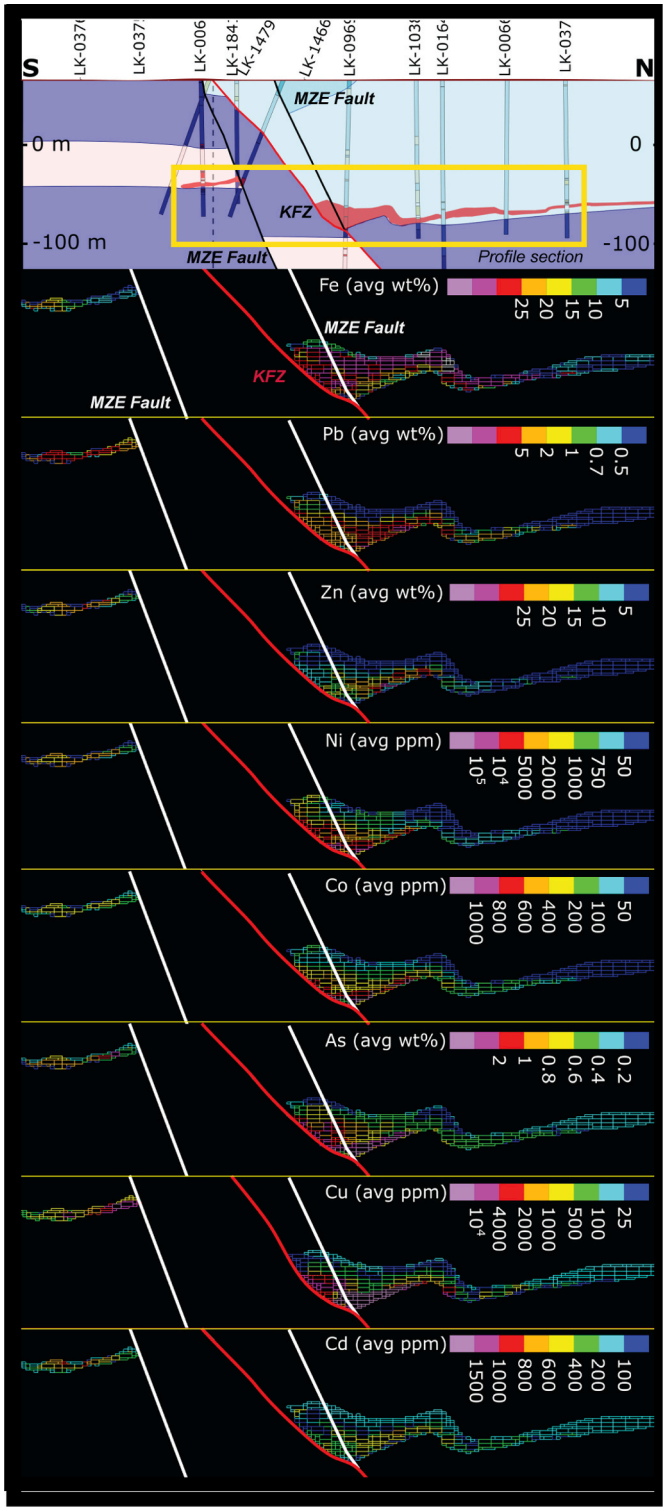


**Fig. 3.** A section through the Lisheen resource block model, along the S-N cross-section in Fig. 2b, showing the average concentrations of Fe, Pb, Zn, Ni, Co, As, Cu and Cd within a given block. Methodology is as in Torremans et al. (2018). Major structures indicated are the Killoran Fault Zone (KFZ; red line) and two segments of the Main Zone East (MZE) Fault (white lines) that have been displaced by the KFZ. The yellow box highlights the exact area of the element maps. (For interpretation of the references to colour in this figure legend, the reader is referred to the web version of this article.)

**Table 1**
Pyrite trace element chemistry data from the Lisduff Oolite Member (LOM)-hosted sulphides. Sample SPL010 is from the Ramp Zone, SPL041A from the Main Zone. Detection limits (DL) are specified at the base of the table. The pyrite samples represented in this table are shown petrographically in Fig. 9.

| Sample ID | Pyrite group | S (wt. %) | Fe (wt. %) | As (wt. %) | Tl (wt. %) | Co (wt. %) | Cu (wt. %) | Ni (wt. %) | Pb (wt. %) | Ag (wt. %) |
|---|---|---|---|---|---|---|---|---|---|---|
| **SPL010** | Py0 | 48.82 | 41.63 | 5.18 | <DL | 0.14 | 0.23 | 0.67 | 1.66 | 0.02 |
| | Py0 | 49.13 | 42.09 | 5.21 | <DL | 0.13 | 0.21 | 0.66 | 0.99 | 0.02 |
| | $Py1_{early}$ | 50.04 | 42.33 | 5.41 | 0.03 | 0.07 | 0.16 | 0.29 | 1.02 | <DL |
| | $Py1_{early}$ | 50.66 | 43.13 | 4.22 | 0.11 | 0.06 | 0.15 | 0.24 | 1.06 | <DL |
| | $Py1_{early}$ | 53.74 | 45.84 | 0.40 | <DL | 0.06 | <DL | <DL | 0.03 | <DL |
| | $Py1_{early}$ | 53.43 | 45.84 | 0.59 | 0.04 | 0.06 | <DL | <DL | 0.03 | <DL |
| | $Py1_{early}$ | 53.48 | 45.60 | 0.69 | 0.08 | 0.04 | 0.02 | <DL | <DL | <DL |
| | $Py1_{early}$ | 54.24 | 46.76 | 0.05 | <DL | 0.08 | 0.01 | <DL | <DL | <DL |
| | $Py1_{early}$ | 54.31 | 46.49 | 0.10 | <DL | 0.07 | <DL | 0.03 | <DL | <DL |
| | $Py1_{early}$ | 54.05 | 46.67 | 0.03 | <DL | 0.06 | <DL | <DL | <DL | <DL |
| **SPL041A** | Py0 | 53.06 | 45.37 | 0.41 | <DL | 0.09 | 0.02 | 0.15 | 0.61 | <DL |
| | $Py1_{early}$ | 52.69 | 44.23 | 1.19 | <DL | 0.21 | 0.05 | 0.15 | 1.07 | <DL |
| | $Py1_{early}$ | 53.46 | 45.58 | 0.62 | <DL | 0.06 | <DL | 0.04 | 0.64 | <DL |
| | $Py1_{early}$ | 53.49 | 45.29 | 0.62 | <DL | 0.07 | <DL | 0.04 | 0.57 | <DL |
| | $Py1_{early}$ | 53.80 | 45.37 | 0.14 | 0.18 | 0.11 | 0.09 | 0.25 | 0.08 | <DL |
| | $Py1_{early}$ | 53.14 | 45.35 | 0.86 | <DL | 0.06 | 0.05 | 0.08 | 0.45 | <DL |
| | $Py1_{early}$ | 53.42 | 45.49 | 0.60 | <DL | 0.08 | 0.02 | 0.03 | 0.40 | <DL |
| | $Py1_{early}$ | 52.52 | 44.69 | 1.09 | <DL | 0.12 | 0.10 | 0.19 | 0.38 | 0.02 |
| | $Py1_{late}$ | 49.12 | 42.12 | 6.38 | 0.29 | 0.17 | 0.20 | 0.31 | 0.93 | 0.02 |
| | $Py1_{late}$ | 49.01 | 41.95 | 6.07 | 0.29 | 0.12 | 0.27 | 0.35 | 1.28 | 0.03 |
| **DL's** | | 0.01 | 0.01 | 0.02 | 0.02 | 0.01 | 0.01 | 0.02 | 0.01 | 0.01 |

<DL = below detection levels.
SPL010: borehole LK-1063 (easting, northing co-ordinates: 219223.13, 166173.13).
SPL041A: borehole LK-201 (easting, northing co-ordinates: 220260.34, 166454.39).

**Table 2**
Sulphur $\delta^{34}S$ values (laser ablation gas mass spectrometry) for Lisduff Oolite Member (LOM)-hosted mineralisation at the Main, Ramp and Derryville zones. Abbreviations used: SO = Steel Ore; Py = Pyrite; Gn = Galena; Sp = Sphalerite.

| Sample ID | Borehole | Depth (m) | Zone | Phase | Group | $\delta^{b}S$ |
|---|---|---|---|---|---|---|
| LSPL088B_1* | Stockpile | N/A | SO – Main | Gn | Gn1 | −4.74 |
| L_SPL088B_3 | Stockpile | N/A | SO – Main | Gn | Gn1 | −5.47 |
| L_SPL088B_2 | Stockpile | N/A | SO – Main | Py | $Py1_{early}$ + mrc? | −8.13 |
| LSPL088B_4* | Stockpile | N/A | SO – Main | Py | $Py1_{early}$ + mrc? | −7.44 |
| L_SPL037_1 | LK-159 | 164.6 | Main | Py | Py0 | −28.38 |
| L_SPL037_2* | LK-159 | 164.6 | Main | Py | Py0 | −26.3 |
| L_SPL013_1 | LK-479 | 164.5 | Main | Py | $Py1_{early}$ | −15.78 |
| L_SPL013_2 | LK-479 | 164.5 | Main | Py | $Py1_{early}$ | −17.03 |
| L_SPL013_3 | LK-479 | 164.5 | Main | Py | $Py1_{early}$ | −19.38 |
| L_SPL086_2* | Stockpile | N/A | Main | Py | $Py1_{early}$ | −12.25 |
| L_SPL025_4 | LK-1118 | 172.75 | Main | Gn | Gn2 | −2.51 |
| L_SPL025_2* | LK-1118 | 169.75 | Main | Sp | Sp2 | 1.58 |
| L_SPL025_3 | LK-1118 | 169.75 | Main | Sp | Sp2 | 0.36 |
| L_SPL040_2 | LK-201 | 243.25 | Ramp | Py | Py0 | −23.79 |
| L_SPL041A_1 | LK-201 | 244.05 | Ramp | Py | Py0 | −21.93 |
| L_SPL041A_2 | LK-201 | 244.05 | Ramp | Py | Py0 | −23.42 |
| L_SPL046B_1 | LK-310 | 344.3 | Ramp | Gn | Gn2 | −3.37 |
| L_SPL046B_5 | LK-310 | 344.3 | Ramp | Gn | Gn2 | −1.9 |
| L_SPL040_1* | LK-201 | 243.25 | Ramp | Sp | Sp1 | −7.31 |
| L_SPL040_3* | LK-201 | 243.25 | Ramp | Sp | Sp1 | −12.04 |
| L_SPL040_4* | LK-201 | 243.25 | Ramp | Sp | Sp1 | −6.99 |
| L_SPL046B_2 | LK-310 | 344.3 | Ramp | Sp | Sp1 | 0.66 |
| L_SPL046B_3 | LK-310 | 344.3 | Ramp | Sp | Sp1 | −3 |
| L_SPL046B_4 | LK-310 | 344.3 | Ramp | Sp | Sp1 | −1.57 |
| L_SPL092_1 | Stockpile | N/A | Derryville | Py | $Py1_{early}$ | −25.31 |
| L_SPL089_1 | Stockpile | N/A | Derryville | Gn | Gn2 | −2.9 |
| L_SPL092_2* | Stockpile | N/A | Derryville | Gn | Gn1 | −13.96 |
| L_SPL092_4 | Stockpile | N/A | Derryville | Gn | Gn1 | −9.21 |
| L_SPL092_3 | Stockpile | N/A | Derryville | Sp | Sp1 | −7.1 |
| L_SPL092_6 | Stockpile | N/A | Derryville | Sp | Sp1 | −7.85 |
| L_SPL092_7 | Stockpile | N/A | Derryville | Sp | Sp1 | −8.83 |
| L_SPL089_2 | Stockpile | N/A | Derryville | Sp | Sp1 | −7.19 |

*denotes a $\delta^{34}S$ isotope value previously published in Yesares et al. (2019).
Borehole northing and easting co-ordinates:
• LK-159: 219479.14, 166170.94 • LK-479: 219539.81, 166170.11 • LK-1118: 219253.02, 166158.24 • LK-201: 220260.34, 166454.39 • LK-310: 220335.33, 166516.05.
Stockpile samples are from unknown co-ordinates, with their general location provided by Güven pers. comm. (2020).

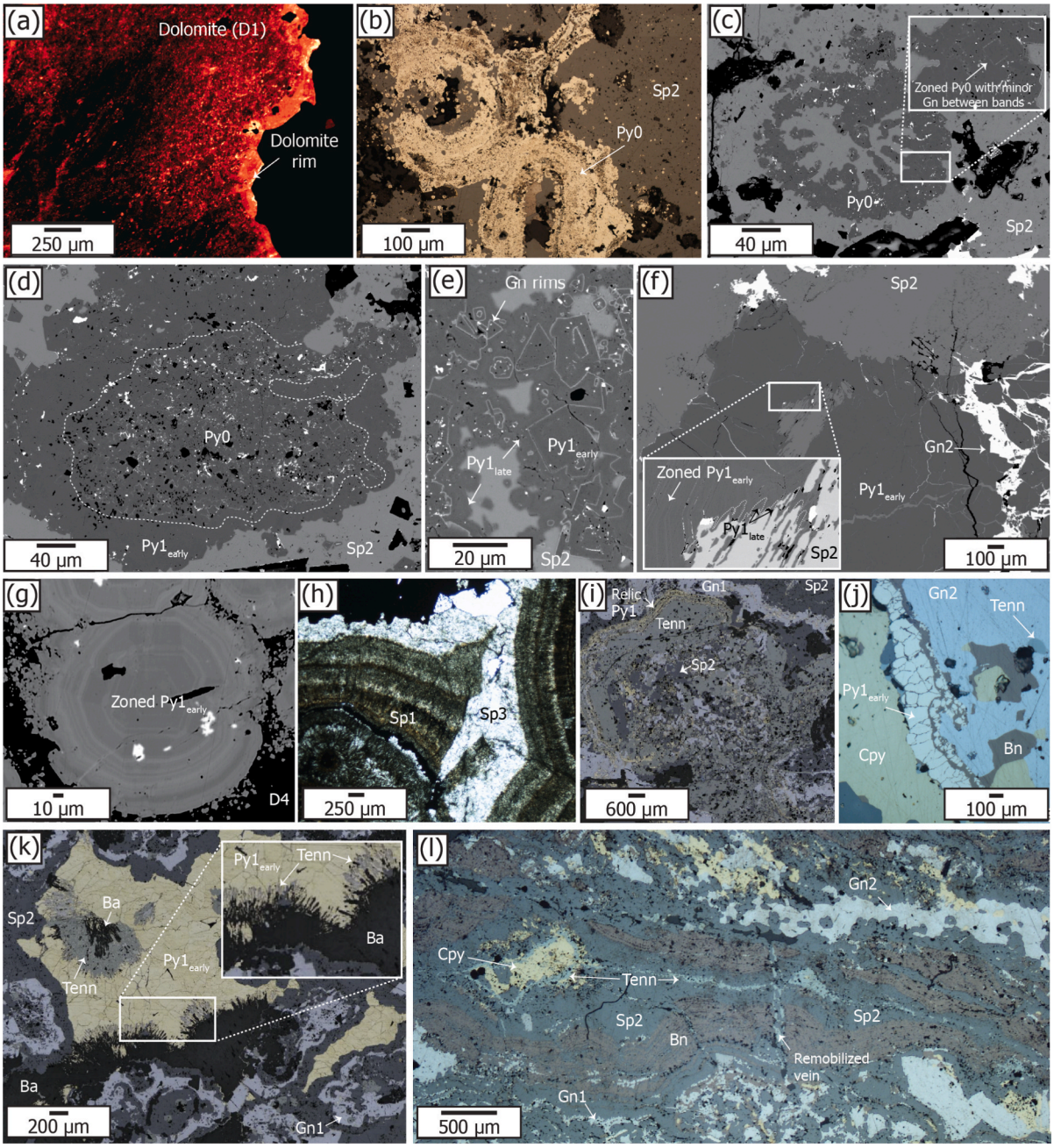


**Fig. 4.** Key ore textures and sulphide phases from LOM-hosted mineralisation in the Lisheen deposit. (a) Cathodoluminescence (CL) image of dolomitised (D1) LOM, with subsequent dolomite rims growing on the margin of open space (featureless dark area on the right hand side of the image). Minor sulphide specks are seen throughout (non luminescent spots). (b) Reflected light micrograph of pyrite (Py0) replacement of oolitic textures, with subsequent sphalerite (Sp2) replacement. (c) SEM image of Py0, after bioclastic shell fragment. This image shows dissolution-reprecipitation textures, where pyrite infills space left after dissolution of the original shell fragment. A magnified inset image shows minor galena between pyrite bands. (d) SEM image of Py0, which is inclusion rich, overgrown by $Py1_{early}$. (e) SEM image of $Py1_{early}$ clasts overgrown by $Py1_{late}$, with later replacement and infilling by Sp2. (f) SEM image of $Py1_{early}$ replaced by Sp2 and cut by galena infilled (Gn2) fractures. The inset box shows Sp2 replacing $Py1_{late}$, which had previously veined and replaced $Py1_{early}$. $Py1_{early}$ displays texturally zoned morphology. (g) SEM image of texturally zoned $Py1_{early}$ surrounded by later dolomite. (h) Transmitted light micrograph of colloform sphalerite (Sp1) cut by late, pale sphalerite (Sp3). (i) Reflected light micrograph of $Py1_{early}$ relicts within a Sp2-Tenn mass, with Gn1 that has replaced Sp2. (j) Reflected light image of early pyrite, with chalcopyrite (Cpy), bornite (Bn) and Gn2. (k) Reflected light micrograph of coarse, sometimes zoned $Py1_{early}$ replaced by Sp2. Sp2 was in turn replaced by galena (Gn1) and tennantite (Tenn). Barite (Ba) is also present and appears to infill open space with some needle-like growths (inset). The direct relations and timing between Ba and these other minerals are unclear, but tennantite and sphalerite are closely associated. (l) Reflected light micrograph of Sp2 replaced by Gn1; Gn1 and Tenn are also veined by Sp. Cpy infills cavities and is associated with the brecciation of Gn1. Bornite selectively replaces Sp2. There is a late vein infilled with remobilized Sp2, Tenn and Cpy. Modified from Lyons (2019). (m) Paragenesis of LOM-hosted mineralisation located in the Main, Ramp and Derryville ore zones. Post-ore minor phases are based on observations by Lyons (2019)
Adapted from Lyons (2019).

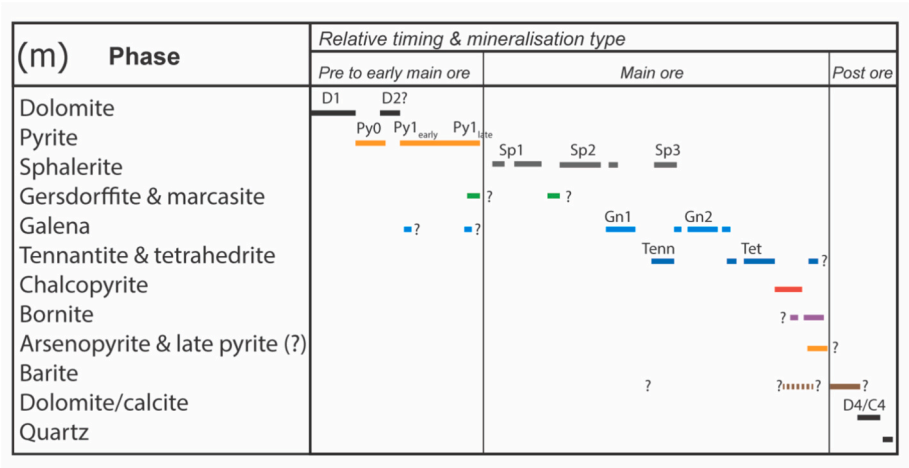


**Fig. 4.** (*continued*).

## 4. Results

### 4.1. Mineralogy and paragenetic relations

Lisduff Oolite Member-hosted mineralisation has a sulphide assemblage consisting mainly of pyrite, galena and sphalerite, accompanied by non-sulphides barite, dolomite, and calcite. Minor chalcopyrite, marcasite, bornite, arsenopyrite, nickeline/niccolite (NiAs), gersdorffite (NiAsS), tennantite-tetrahedrite ($Cu_{12}As_4S_{13}$-$Cu_{12}Sb_4S_{13}$) and possibly bravoite ((FeNiCo)S) are also present. Locally, accessory quartz and unidentified aluminosilicate phases occur as small inclusions or infilling small vugs (generally < 50 μm).

While limited, previously described LOM-hosted mineralisation in the Rathdowney Trend has been associated with dolomitised LOM intervals (e.g., Eyre, 1998). Dolomitisation was associated with the dissolution of the host rock, including oobiosparites and oosparites, with additional dolomite found on the margins of these cavities (Fig. 4a). Following dolomitization, several generations of pyrite, sphalerite, galena and chalcopyrite were precipitated. Detailed textural and paragenetic descriptions are presented in the following sections. The first section presents the majority of LOM-hosted mineralisation (Fig. 4), excluding the area referred to as steel ore. The second section presents steel ore mineralisation, which displays more significant replacement features and Ni-phases (Fig. 5).

*Main, Ramp and Derryville zones (excluding steel ore):* Pyrite is the earliest, and most ubiquitous, mineral phase in the Main, Ramp, and Derryville zones. Pyrite mineralisation has been classified into two groups based on distinctive textures in each group: Py0 and Py1 (Fig. 4b-c, Fig. 4d-g, respectively). A further subdivision based on relative paragenetic stage is included for Py1: $Py1_{early}$, and $Py1_{late}$. Py0 is inclusion-rich, has some zonation, replaces the host rock, and often preserves original oolitic spheroids (Fig. 4b) or bioclastic (Fig. 4c) fragments through dissolution and reprecipitation mechanisms (typically < 200 μm – 2 mm). $Py1_{early}$ may occur as overgrowths of variable thickness on Py0 (e.g., Fig. 4d; <2–50 μm), with more complex morphologies typically observed within Main Zone samples. More typical growth of $Py1_{early}$ occurs as coarsely (>1 mm) zoned/banded (e.g., Fig. 4d-g, Fig. 9a), inclusion-free forms. $Py1_{early}$ may also occur as weakly zoned, euhedral grains of pyrite (e.g., Fig. 4e, g). There are sometimes thin galena rims between $Py1_{early}$ and $Py1_{late}$ forms (e.g., Fig. 4e). $Py1_{late}$, which forms paragenetically later than $Py1_{early}$, often displays less defined / more chaotic shapes, overgrowing (Fig. 4e) or replacing (e.g., Fig. 4f) earlier $Py1_{early}$. This replacement feature can be seen by the $Py1_{late}$ that cross-cuts the growth bands of $Py1_{early}$ in the inset image of Fig. 4f. The textures associated with $Py1_{late}$ are extremely variable, and are often more chaotic in areas adjacent to feeder fault zones (e.g., Fig. 9b).

The main ore stage mineralisation includes sphalerite, galena, and Fe- and Cu-bearing phases. There are three generations of sphalerite (Sp1-3), defined by colour variation in transmitted light and textural associations with other minerals (e.g., Fig. 4h). Sp1 is typically dark reddish-brown, precipitated as vug infill, and/or overgrew earlier pyrite. It occurs as coarse colloform masses and has lighter colours in outer growth zones. Small intergrowths of galena (>~1 mm) are locally found between Sp1 colloform bands. Medium to dark brown Sp2 often replaces earlier pyrite (e.g., Fig. 4f). Sp3 is more coarsely crystalline (>0.5 mm), and inclusion free than previous sphalerite generations. Sp3 displays wide colour variability, with clear/colourless, to pale yellow, to medium brown forms identified. While observed infilling open space, colourless forms of Sp3 are noted cross-cutting earlier sphalerite phases (e.g. Sp1; Fig. 4h).

Most galena either replaces Sp2 that has previously replaced pyrite (Gn1; Fig. 4i) or it occurs as vein or open space infill (<100 μm to > 1 mm) (Gn2; Fig. 4f). Tennantite post-dates galena and replaces, or is hosted by veins and vugs within, earlier phases (Fig. 4i-l). It typically replaces Sp1, Sp2 (generally > 2 mm; Fig. 4i) and galena, or cross-cuts bornite within late remobilisation veins (e.g., 4 l). Tennantite is more abundant in the Derryville Zone samples, along with chalcopyrite and bornite (Fig. 4j, l), occurring as veins and/or space infill. Bornite is observed selectively replacing colloform sphalerite bands (e.g., Fig. 4l). Chalcopyrite replaces minor amounts of $Py1_{early}$ and infills vugs within earlier sulphides (Fig. 4l). Exact timing relationships of bornite are not clear, but it appears to have intergrown with chalcopyrite in places. Arsenopyrite is not common within LOM-hosted samples, but when present occurs as small infill or minor euhedral crystals (<10 μm) as shown in Fig. 5i from the steel ore region.

Other mineral phases include barite, carbonates and quartz. While the observation of barite is limited in this study, when identified, it occurs as infill or lath-like growth on the margins of earlier phases (Fig. 4k). Exact relationships between barite and sulphides are unclear, meaning exact timing of growth is also uncertain, but barite is closely associated with sphalerite and tennantite in some LOM-hosted samples (Fig. 4k). Dolomite/calcite are present as late veins, and open space infill (see C4 and D4 from Wilkinson et al., 2005). Minor late pyrite (<1 μm) is also present in small amounts. Quartz, in late veinlets <~0.5 mm that crosscut dolomite, is noted in parts. Quartz is present in minor amounts with unclear paragenetic relations to most phases other than dolomite (e.g., Lyons, 2019). Paragenetic relationships of LOM-hosted mineralisation are summarised in Fig. 4m.

*Steel ore mineralisation:* The steel ore mineralisation has similar paragenetic relationships to other LOM-hosted mineralisation. However, there is relatively more galena present within the steel ore region.

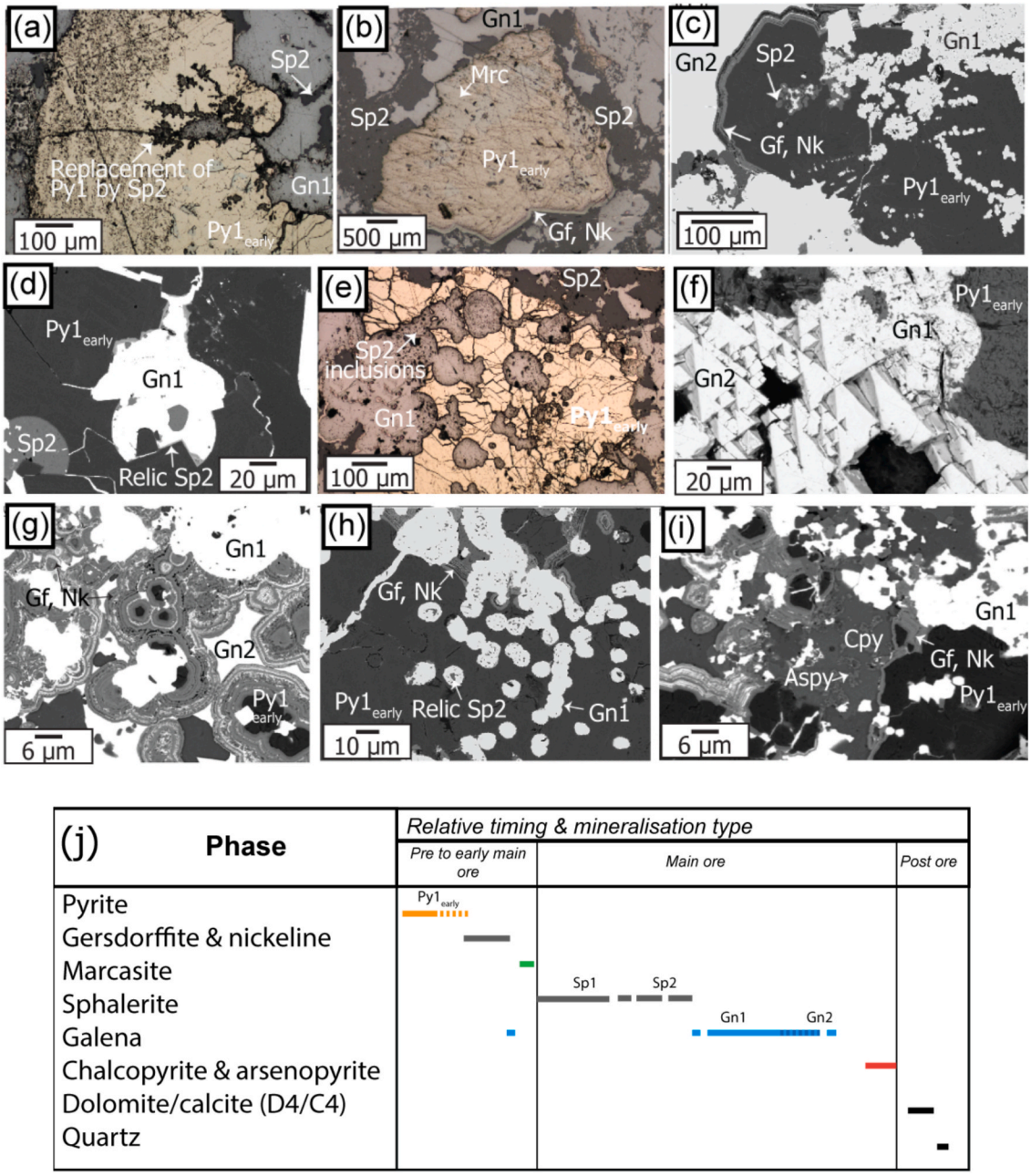





**Fig. 5.** Key ore textures and sulphide phases from steel ore-hosted mineralisation. (a) Reflected light micrograph showing $Py1_{early}$ with apparent skeletal sphalerite (Sp2), formed by replacement of the $Py1_{early}$. Additional Sp2, that originally nucleated on $Py1_{early}$ (relicts on margins of Gn1), was subsequently infilled and partially replaced by galena. (b) Reflected light micrograph of $Py1_{early}$ replaced by Mrc and overgrown by nickeline (Nk) and gersdorffite (Gf). Gn1 is also replacing Sp2. (c) SEM image of $Py1_{early}$ replaced by Sp2, which is replaced by Gn1. (d) SEM image showing relict Sp2 within Gn1, both replacing $Py1_{early}$. (e) Reflected light micrograph of Gn1 replacing Sp2 (full of Sp2 inclusions), associated with $Py1_{early}$. The thin band of pyrite associated with Gn1 in the bottom left of the micrograph represents a relict of $Py1_{early}$ that was partially replaced by Sp2, that was subsequently replaced by the Gn1. (f) SEM image of replacement Gn1 and interstitial Gn2. (g) SEM image of banded Nk, Gf, nucleating on $Py1_{early}$ crystals. Gn1 replaces all these minerals and is overgrown by interstitial Gn2. (h) SEM image showing inclusions of Sp2 within Gn1, replacing $Py1_{early}$. (i) SEM image of late Cpy with euhedral arsenopyrite (Aspy) cutting Nk, Gf and Gn1. The Nk-Gf nucleated on $Py1_{early}$. (j) Paragenesis of the steel ore area of the Main Zone LOM-hosted mineralisation. Post-ore minor phases are based on observations by Lyons (2019).

Pyrite is also present with textures overlapping those of paragenetically similar phases elsewhere in the LOM (Fig. 5a); however Py0 and thin bands of $Py1_{early}$ growth bands were not observed in the steel ore area. In addition, minor marcasite is observed in association with $Py1_{early}$ (Fig. 5b). While marcasite-pyrite relations are unambiguous, it appears that marcasite is cementing brecciated pyrite. Both are overgrown by very thin bands (<5 µm) of nickeline and gersdorffite (Fig. 5b, c), with minor galena. Banded gersdorffite is cut by Sp2 similar to LOM-hosted mineralisation, but is more abundant in steel ore. (Similar banded nickeline and gersdorffite textures are observed in one sample from the Derryville Zone, but they are generally more extensively developed in the steel ore region than elsewhere.) Extensive replacement of pyrite by sphalerite (Sp2) (e.g., Fig. 5a, d-e) is observed throughout the steel ore region. Galena occurs as both replacive (Gn1; Fig. 5d, f-h) and infilling (Gn2; Fig. 5f, i) forms, with Gn1 preferentially replacing Sp2. Minor late chalcopyrite and arsenopyrite (Fig. 5i) are observed in the steel ore, along with infrequent dolomite and quartz. Paragenetic relationships of LOM-hosted steel ore mineralisation are summarised in Fig. 5j.

### 4.2. Mineral chemistry: results

*Main, Ramp and Derryville zones (excluding steel ore):* Major and minor element analysis of pyrite from the LOM are presented in Figs. 6-8, by location across the mine and by paragenetic phase. All associated data are provided in the electronic supplementary material (ESM) 1, including detection limits. Similar trends for Fe and S are seen for all pyrite types (Py0, $Py1_{early}$, $Py1_{late}$; Fig. 6a) within LOM-hosted samples, with **Py0** (n = 50) having variable concentrations of As (mean, median of 2.13 wt%, 0.91 wt%; range 0.03–6.1 wt%), Tl (0.04–0.31 wt%), Ni (0.03–0.32 wt%), Co (0.04–0.09 wt%), Cu (mean, median 0.07 wt%, 0.03 wt%; range 0.02–0.1 wt%), and Pb (0.02–0.69 wt%). Other elements (Bi, Mn, Ag) are typically at or below detection limits (<0.01 wt %). Py0 displays a strong negative correlation between S and As (−0.92 using Pearson correlation coefficient, $r^2 = 0.85$; Fig. 6b), and a slightly weaker correlation between Fe and As (−0.85, $r^2 = 0.73$; Fig. 6c). Trace elements hosted by Py0 (Ag-Pb-Ni-Tl and Co-Ni) display weak positive correlations (~0.6–0.7) with one another.

**$Py1_{early}$** (n = 267) displays somewhat lower mean and median values for As (0.96 wt%; 0.48 wt%) and Cu (0.04 wt%; 0.03 wt%) (ranges 0.03–2.66 wt%, 0.02–0.06 wt%, respectively) relative to Py0. Within $Py1_{early}$, Pb displays widely variable values (0.02–1.71 wt%; mean and median values of 0.38 wt% and 0.24 wt%, respectively). $Py1_{early}$ displays similar ranges for Tl (0.03–0.35 wt%), Ni (0.03–0.31 wt %), and Co (0.04–0.11 wt%), relative to Py0. $Py1_{early}$ contains small amounts of Ag (0.01–0.03 wt%) and Mn (0.02–0.06 wt%). Arsenic data for $Py1_{early}$ also display negative correlations with S (−0.88, $r^2$ value of 0.77; Fig. 6b) and Fe (−0.78, $r^2$ value of 0.6; Fig. 6c). While $Py1_{early}$ data reveal a weak positive correlation between As and Tl (+0.6; Fig. 6d) and between Cu and Ni (+0.69), no significant trends can be observed.

**$Py1_{late}$** (n = 22) generally shows elevated mean concentrations (Fig. 8) relative to **$Py1_{early}$**, along with elevated mean and median Pb values (0.79 wt% and 0.89 wt%, respectively; range 0.06–1.52 wt%), Cu (0.02–0.53 wt%), Ni (0.03–1.02 wt%), and Co (range 0.05–0.42 wt%). $Py1_{late}$ hosts As (mean, median 3.53 wt%, 2.74 wt%; range 0.23–6.91 wt %) and Tl (0.03–0.39 wt%) ranges similar to Py0 (Fig. 6d), and Ag (0.02–0.05 wt%) contents similar to $Py1_{early}$. However, $Py1_{late}$ has higher mean values for As, with As displaying stronger negative

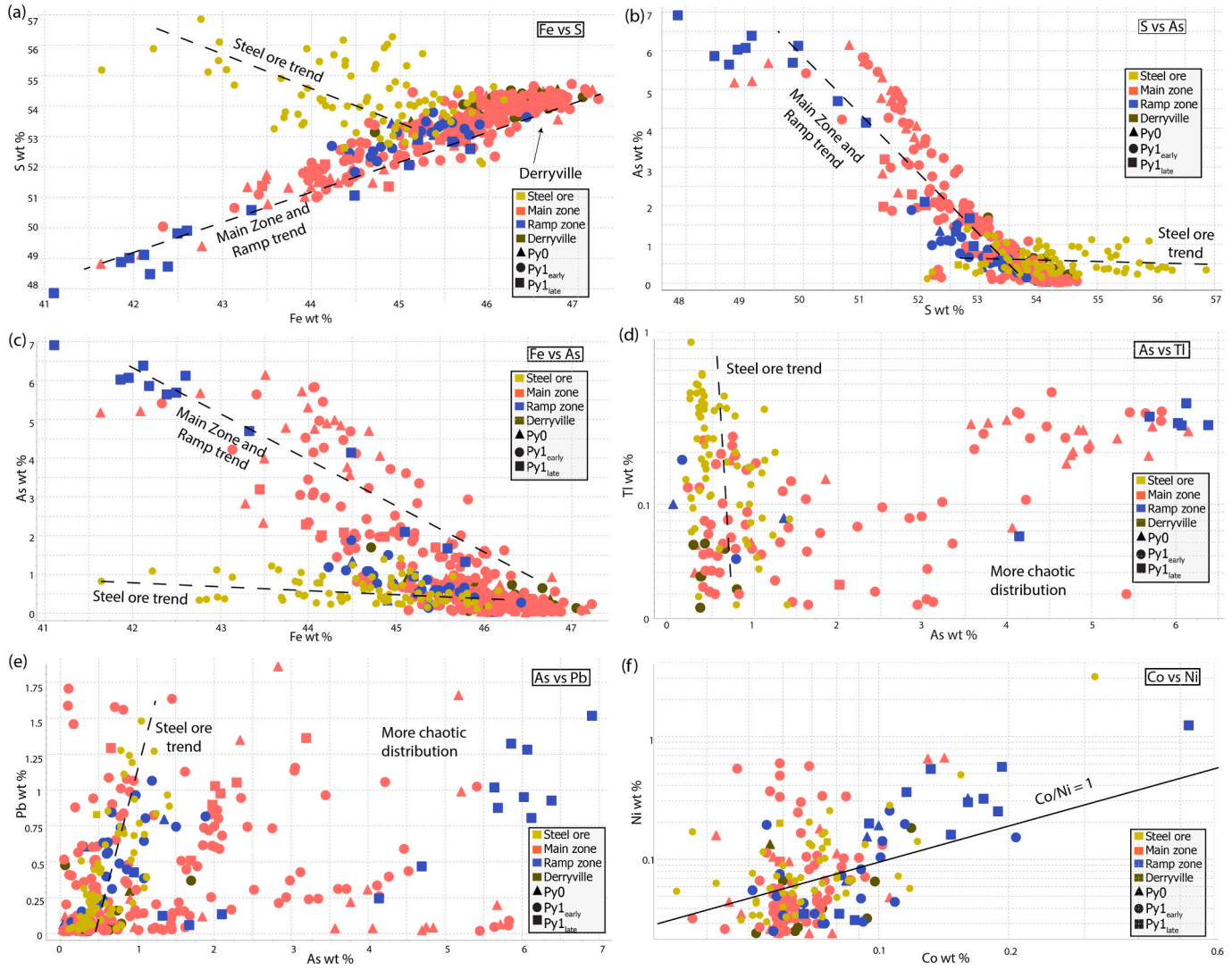


**Fig. 6.** Selected bivariate plots for pyrite from LOM- and steel ore-hosted mineralisation across the Lisheen deposit. Trendlines for both LOM and steel ore samples are shown by dashed lines, where relevant. All pyrite phases (Py0, $Py1_{early}$, $Py1_{late}$) studied are included in the plots. **(a)** Plot of Fe and S. Trends for steel ore and ramp regions are highlighted showing decreasing Fe and S with pyrite phase in the ramp region. **(b)** S and As plot revealing elevated As in $Py1_{late}$ ramp samples, and elevated levels of S in several steel ore samples. **(c)** Plot of Fe and As, showing similar patterns to S and As in (b), with the steel ore samples displaying a different trend. **(d)** Plot of As and Tl, showing high Tl variability in steel ore samples, while the rest of the samples display more variable trends. **(e)** As and Pb plot displaying lack of correlation, except in steel ore where there is a positive correlation. **(f)** Plot of Co and Ni, where Co/Ni = 1 is shown for reference (see text for discussion).

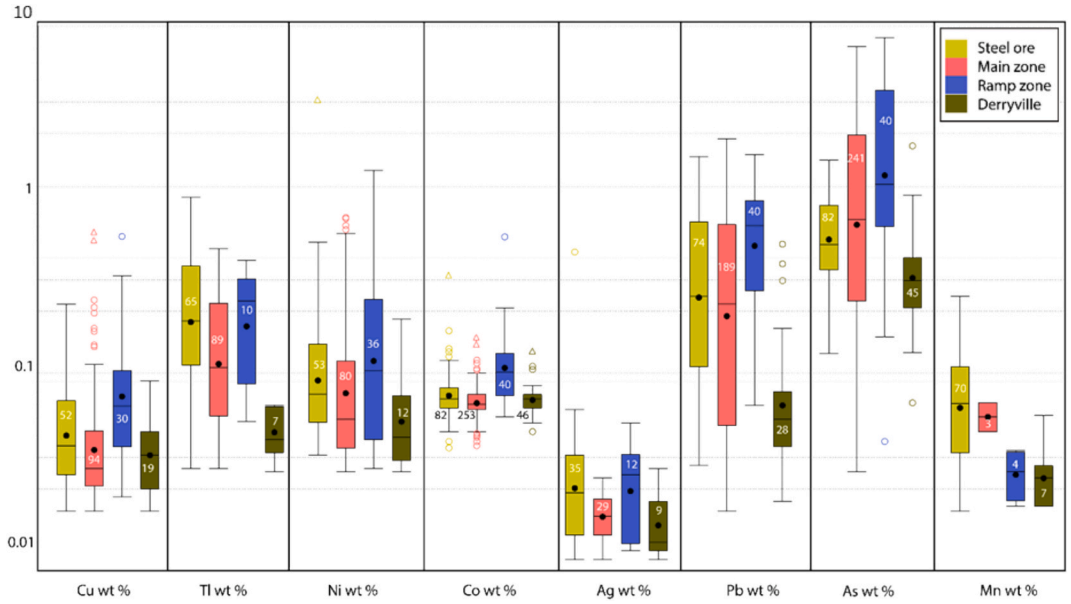


**Fig. 7.** Box plot of select elements from all pyrite phases, defined by location across LOM-hosted mineralisation. This plot is to showcase the generalised trends across ore zones, as a comparative tool. The steel ore pyrite has elevated concentrations of most elements, with notably high Mn, relative to other locations. The Ramp Zone hosts the highest median concentrations of most elements, except for Mn. The Derryville Zone pyrite has the lowest concentrations of all elements. Whiskers represent minimum and maximum values, while the bottom and top of each box relate to the Q1 and Q3 values respectively. The median is depicted by the line, while the black dot represents the mean values for each phase. The number of samples analysed (n) is shown for each phase.

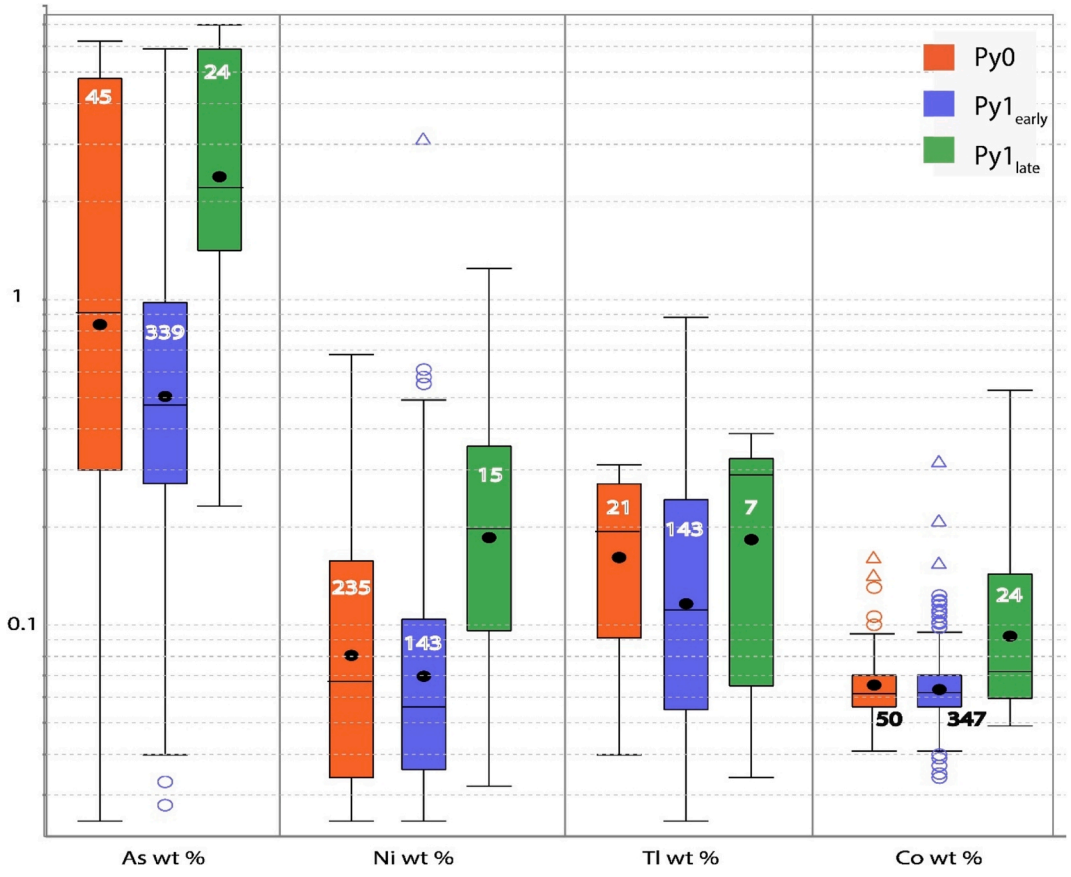


**Fig. 8.** Box plot of As, Ni, Tl and Co data for Py0, $Py1_{early}$, $Py1_{late}$, including steel ore-hosted samples. Py0 is elevated relative to $Py1_{early}$ in all elements, while $Py1_{late}$ hosts the highest concentrations of each. Whiskers represent minimum and maximum values, while the bottom and top of each box relate to the Q1 and Q3 values respectively. The median is depicted by the line, while the black dot represents the mean values for each phase. The number of samples analysed (n) is shown for each phase.

correlations with both S (−0.97, $r^2$ value of 0.94; Fig. 6b) and Fe (−0.95, $r^2$ value of 0.9; Fig. 6c) than $Py1_{early}$. Arsenic displays a bimodal concentration distribution across pyrite phases, with most values ranging between 4 to 6.5 wt% for Py0, initial $Py1_{early}$ bands and $Py1_{late}$, while As concentrations in coarse $Py1_{early}$ are typically below < 1.5 wt%.

*Steel ore mineralisation:* Within the steel ore, Py1 is the dominant pyrite type analysed ($Py1_{early}$ (n = 80) and $Py1_{late}$ (n = 2)). As $Py1_{early}$ was by far the more common phase recorded, with more data available, this is the focus of descriptions. $Py1_{early}$ displays variable ranges for several elements, especially when compared to other LOM zones (Fig. 6). Within the steel ore, As ranges from 0.12-1.42 wt% (mean, median of 0.58 wt%, 0.47 wt%), Mn ranges from 0.02-0.22 wt%, Ag ranges from 0.01-0.05 wt%. Arsenic and Pb display a positive correlation of 0.68 (Fig. 6e), whereas there is a negative correlation between Pb and Tl (−0.55 correlation coefficient). In contrast to pyrite in other LOM zones, data from the steel ore does not reveal any correlations between either S or Fe and other elements analysed. Cobalt and Ni values from all pyrite types in this mineralisation have Co/Ni values both greater and less than 1 (<1n = 80, and > 1n = 128; Fig. 6f).

**Galena** from the steel ore area was also studied from two samples (SPL088 and SPL088A; n = 24) including both Gn1 and Gn2, and they have variable S/Pb values. Replacive **Gn1** (n = 16) has low levels of several trace elements, including Zn (0.10 – 0.12 wt%), Fe (0.03 – 0.3 wt %), As (0.02 – 1.2 wt%), Cu (0.01 – 0.3 wt%), and Ni (0.01 – 0.13 wt%). Infilling **Gn2** (n = 8) displays overlapping ranges for all of these elements, but generally has lower trace element abundances.

### 4.3. Comparison of LOM-hosted mineralisation zones

To consider the trace element results from a broader viewpoint, data from all pyrite phases have been merged for review across ore zones by box plots (Fig. 7). This is in part to help view the data for an exploration point of view, where detailed paragenetic relations may not be constrained. While there is overlap in element distributions, there are differences in median concentrations between the different LOM-hosted mineralised zones (Fig. 7; see Fig. 2 for relative locations). Median values of Cu, Tl, As, Ni, Co, Ag and Pb in pyrite are highest in the Ramp Zone, with slightly lower values in Main Zone; the Derryville Zone has the lowest values. Steel ore samples generally overlap with those from Main Zone, with slightly elevated median values (Fig. 7), but As-Tl-S-Fe data display different trends than other LOM-hosted mineralisation (Fig. 6a-d). Spatially, Cu, Tl, As, Co and Ni show a relative decrease in median value from the steel ore to the adjacent Main Zone mineralisation, whereas As is slightly elevated in the Main Zone (Fig. 7). Mn shows elevated values in Main Zone, including the steel ore, compared to other zones (Fig. 7), though this observation is based on a small data set and may not be fully representative.

Despite sample collection from various LOM zones to test spatial distributions of elements in pyrite, no clear spatial variations or trends are seen within individual LOM zones. There are also no strong chemical variations between differing pyrite generations from all sample locations. However, Fe, S and As contents in pyrite correlate with minor trace elements (e.g., Tl, Ni, Co; Fig. 8). All elements shown display similar trends, with median As, Ni, Tl and Co values elevated relative in $Py1_{late}$ compared to $Py1_{early}$.

*Variation on a grain scale:* two samples (n = 20; SPL010 and SPL041A) were examined to explore the impact of replacement and overprinting on earlier phases. Sample SPL010 contains Py0 that has been partially replaced and overgrown by thin, initial $Py1_{early}$ bands, followed by later coarse $Py1_{early}$ growth (Fig. 9a). SPL041A comprises Py0 overgrown by $Py1_{early}$ with successive $Py1_{late}$ development (Fig. 9b). $Py1_{late}$ is extensively developed in SPL041A as aggregated masses and infill textures, with thinly banded forms nucleating off earlier $Py0/Py1_{early}$. Early forms of $Py1_{early}$ from SPL010 are generally enriched in As, Cu and Ni (up to 5.4, 0.2 and 0.3 wt%, respectively) relative to later $Py1_{early}$ growth, with both phases containing low levels of Co and Tl (<0.1 wt%). $Py1_{late}$ (n = 2) contains the highest concentrations of As, Cu and Tl from these samples (6.4, 0.3 and 0.4 wt%, respectively) but because only two analyses were obtained this result must be interpreted with caution. Intragrain variation reveals variable trace element distributions, with no observed systematic changes between successive bands of texturally zoned $Py1_{early}$, as was observed in the Island Pod orebody (Doran et al., 2022).

### 4.4. Sulphur isotope results

Sulphur isotope analysis of pyrite, galena, and sphalerite in the LOM-hosted mineralisation have $\delta^{34}S$ values that range from −28.4 to + 1.6 ‰ (n = 32). Data are summarised in Fig. 10a-b, with the full dataset listed in Table 2, while previously collected sulphur isotope data from LOM-hosted mineralisation in Lisheen is summarised in Fig. 10c (data from Hitzman, 1993; Wilkinson et al., 2005; Turner, 2019).

Pyrite from the LOM yields the lowest $\delta^{34}S$ values from the study, with Py0 (−28.4 to −21.9 ‰; n = 5) having lower $\delta^{34}S$ values than $Py1_{early}$ (−25.3 to −7.4 ‰; n = 7). Sphalerite $\delta^{34}S$ values are variable, with Sp1 (−12.0 to + 0.7 ‰; n = 10) and Sp2 (0.4 and 1.6 ‰; n = 2) both yielding generally heavier isotopic compositions than earlier Py. Galena values are typically heavy relative to pyrite, but consistently < 0 ‰ (replacive Gn1 ranges from −14.0 to −4.7 ‰, n = 4; infilling Gn2 ranges from −3.4 to −1.9 ‰, n = 4). Data are described by location at Lisheen below.

**Main Zone** pyrite (Py0 and $Py1_{early}$; n = 6) $\delta^{34}S$ values range from −28.4 to −12.3 ‰, whereas a single galena (Gn2) yields a $\delta^{34}S$ value of −2.5 ‰ and sphalerite (Sp2; n = 2) reveals $\delta^{34}S$ values of + 0.7 and 1.6 ‰.

**Derryville Zone** pyrite ($Py1_{early}$; n = 1) exhibits a $\delta^{34}S$ value of −25.3 ‰, with galena (Gn1 and Gn2; n = 3) and sphalerite (Sp1; n = 4) $\delta^{34}S$ values ranging from −14.0 to −2.9 ‰ and −8.8 to −7.1 ‰, respectively.

**Ramp Zone** mineralisation exhibits $\delta^{34}S$ values of −23.8 to + 0.7 ‰. Pyrite (Py0; n = 3) $\delta^{34}S$ values range from −23.8 to −21.9 ‰, while galena (Gn2; n = 2) have sulphur isotope signatures of −3.4 and −1.9 ‰. Sphalerite (Sp1; n = 6) ranges from −12.0 to + 0.7 ‰.

**Steel ore** pyrite ($Py1_{early}$; n = 2) and galena (Gn1; n = 2) from the Main Zone have $\delta^{34}S$ values of −8.1 to −4.7 ‰. These are the highest values collected in this study. No data are available for steel ore sphalerite, due to its scarcity in this mineralisation style.

Direct comparison between S isotope and trace element data is hindered due to limited overlap in samples, except for $Py1_{early}$ within three samples (SPL041A, SPL013, SPL091). While no direct, spot-for-spot comparison is possible from the current dataset, average Ni, Pb, Tl, S, and As values for $Py1_{early}$ within these samples systematically decrease with decreasing $\delta^{34}S$, but more targeted work is required to explore this variation.

## 5. Discussion

### 5.1. Hydrothermal evolution of LOM-hosted mineralisation

Irish Zn-Pb deposits reflect the complex interplay between various fluid phases, structural controls and replacement processes at the site of deposition. The LOM-hosted mineralisation provides a unique opportunity to test the role of fluid mixing and sulphide replacement in carbonate-hosted systems, along with study of the evolving hydrothermal system and its associated fluids. In our interpretation of mineral chemistry, we assume that chemical variability of a given mineral is principally controlled by variability in the composition of the fluid from which it precipitated. It has been shown that in concentrically zoned aggregates of diagenetic microscopic pyrite crystals, diffusion processes control chemical variation between zones (Qiu et al., 2024), but this type of control is not known in the post-diagenetic, carbonate replacement environment of the LOM. We also assume that variations in

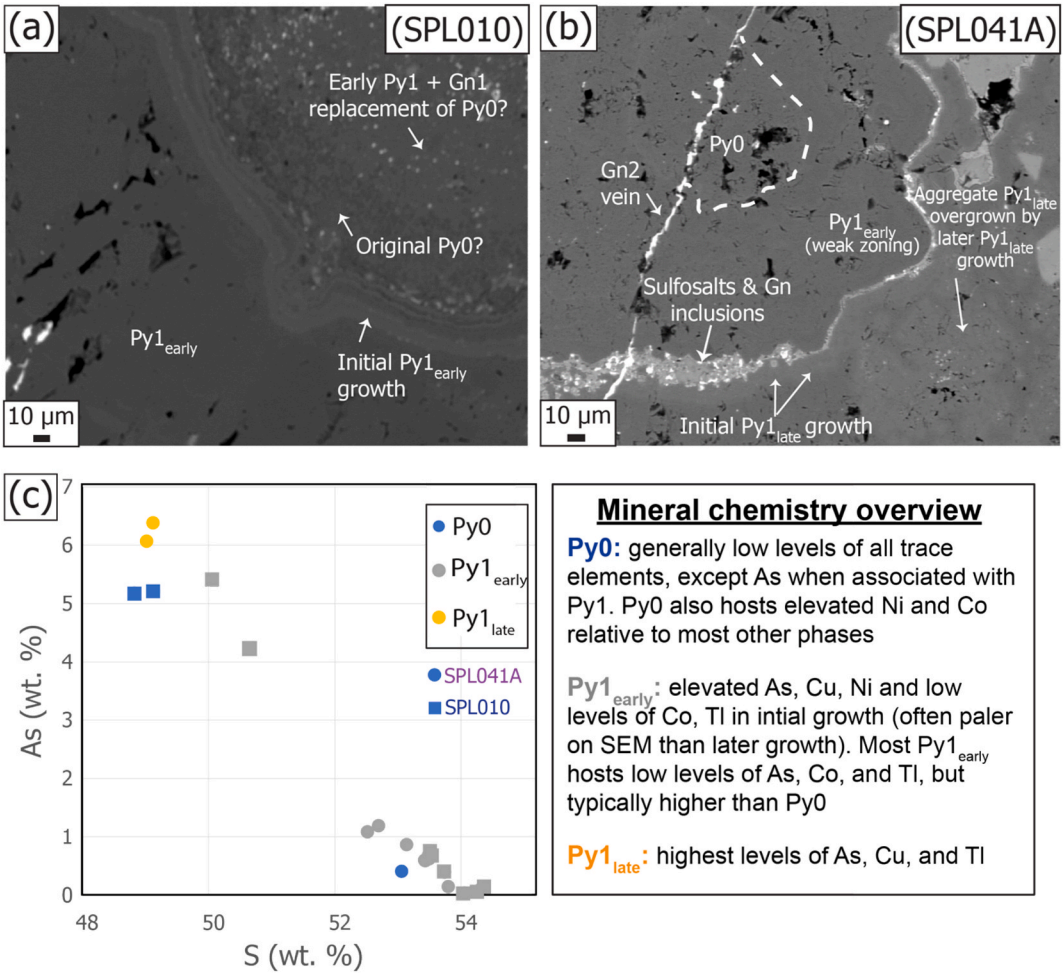


**Fig. 9.** (a) SEM image of pyrite, showing several growth stages. Original Py0 has been partially replaced by initial $Py1_{early}$ (?), with associated minor replacive galena (Gn1). Subsequent thin bands of $Py1_{early}$ overgrow Py0, and in turn are overgrown by later, more massive $Py1_{early}$. Contacts between successive $Py1_{early}$ bands display moderately corrosive margins. (b) SEM image of Py0 overgrown by $Py1_{early}$, with a thin band of gersdorffite and nickeline and minor Gn overgrowing the margins of $Py1_{early}$. $Py1_{late}$ is extensively developed in this sample and it displays complex growth morphologies. Initial $Py1_{late}$ developed as a thin band around gersdorffite, subsequently developing in the surrounding open spaces as small (<10 µm) aggregates. The final succession of $Py1_{late}$ development infills around these earlier forms. A late galena (Gn2) vein cross cuts these earlier phases. (c) Scatter plot displaying As and S EMPA data from samples SPL041A (circles) and SPL010 (squares). There is a strong negative correlation, with elevated As associated with $Py1_{late}$. Py0 from SPL010 hosts elevated As relative to Py0 in SPL041A (Py0 in SPL010 is partially replaced by Py1). Initial $Py1_{early}$ growth in SPL010, as shown in (a) reveals elevated As compared to subsequent $Py1_{early}$ growth. An overview of the EMPA trace element data is also included. Data from these samples is shown in Table 1.

partition coefficient between a given mineral and hydrothermal fluid are not significant controls on mineral composition.

Normal faulting has been shown to play a crucial role in fluid movement and hydrothermal alteration processes at Lisheen, with segmented normal faults connected via relay ramps facilitating fluid migration through an evolving structural framework during ore formation (Hitzman et al., 1992; Shearley et al. 1992, 1996; Earls, 1994; Johnston, 1999; Sevastopulo and Redmond, 1999; Hitzman et al., 2002; Fusciardi et al., 2003; Torremans et al., 2018; Kyne et al., 2019). However, where normal faults intersect (e.g., Main Zone steel ore region; Fig. 2a), our textural and mineralogical data confirm that more complex sulphide assemblages and textures occur, including more extensive and repeated replacement, presumably due to more intense and sustained hydrothermal interactions. In addition, pyrite shows distinct chemical compositional ranges in the steel ore region compared to other LOM-hosted mineralisation (Figs. 6, 7. This could represent an area where hydrothermal fluids initially entered the system, before moving into the rest of the Main Zone orebody. While only a small proportion of the total resource at Lisheen, LOM-hosted mineralisation is mostly found in the structural footwall of main ore-controlling faults (Güven et al., 2023). The LOM is thought to be the first clean carbonate that hydrothermal fluids encountered during migration through fault pathways (Güven et al., 2023), facilitating extensive fluid mixing and replacement.

The Lisheen hydrothermal system has previously been shown to have formed due to mixing of two principal fluids (e.g., Hitzman et al., 2002; Wilkinson et al., 2005; Doran, 2021; Doran et al., 2022). The dual fluid mixing model has been well established across the Irish Zn-Pb orefield, based on several forms of investigation including S isotope data, mineral chemistry and fluid inclusion analysis (e.g., Barrie et al., 2009). The two key sources have been identified as rising metal-rich hydrothermal fluids ($\delta^{34}S$ values typically > 0 ‰) and descending brines carrying bacteriogenically reduced sulphide ($\delta^{34}S$ values typically ~<-25 ‰) (e.g., Boyce et al., 1983a; Anderson et al., 1998; Wilkinson et al., 2005; Barrie et al., 2009; Doran, 2021; Doran et al., 2022). The bacteriogenic origin of sulphur in Irish Zn-Pb deposits like Lisheen is confirmed by extremely light $\delta^{34}S$ values (as low as –47.7 ‰) in early diagenetic pyrite, along with textural and geochemical characteristics (e.g., Boyce et al., 1983a; Wilkinson et al., 2005; Barrie et al., 2009; Doran et al., 2022). Later sulphides with $\delta^{34}S$ values ranging from −25 to + 17.4 ‰

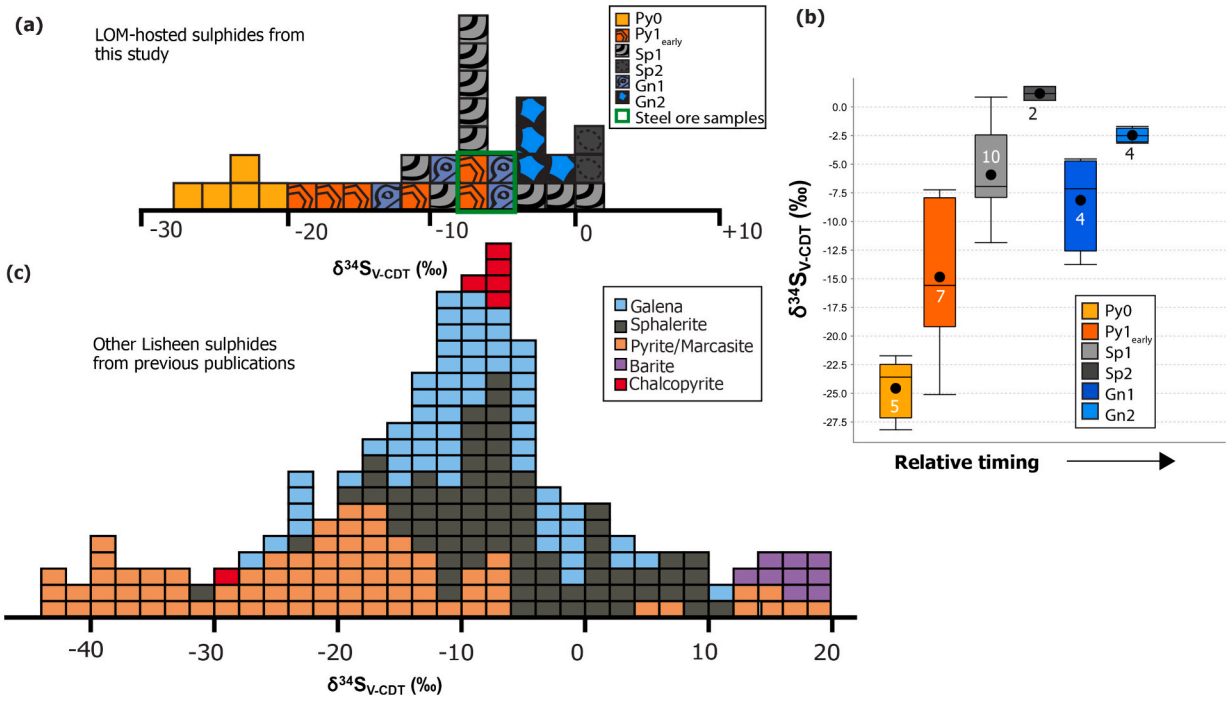


**Fig. 10.** Sulphur isotopic data from LOM-hosted mineralisation across the Lisheen deposit, including previous sulphur isotope work. (a) Histogram of LOM-hosted sulphide $\delta^{34}S$ isotopic values, with each box representing a single data point. (b) Boxplot showing LOM-hosted sulphide $\delta^{34}S$ isotopic data, with relative ore timing. (c) Plot of $\delta^{34}S$ isotopic values from published Lisheen studies. Marcasite (Mrc) and pyrite (Py) are not always separated in published studies and so are all represented by orange boxes. Data is and (For interpretation of the references to colour in this figure legend, the reader is referred to the web version of this article.) adapted from Hitzman et al. (1992), Wilkinson et al. (2005), Turner (2019)Doran et al. (2022).

reflect variable mixing between bacteriogenic brine-derived sulphur and hydrothermal fluid-derived sulphur, as opposed to sulphate reduction in a restricted system which can lead to heavy $\delta^{34}S$ values (e.g., Seal, 2006). If sulphate reduction in a restricted system was responsible, it would be expected that the $\delta^{34}S$ values would show a more progressive, consistent increase with sulphide growth. Consequently, the later sulphides, with $\delta^{34}S$ compositions $>$ 0 ‰, represent the interpreted composition of the hydrothermal end-member (Eyre, 1998; Wilkinson et al., 2005; Doran et al., 2022). Specific $\delta^{34}S$ values and fluid inclusion characteristics vary locally across the orefield, reflecting the variations in fluid sources end-member contributions (Wilkinson and Hitzman, 2014). Variability between S source has also been shown across colloform sphalerite bands at Galmoy, where successive bands can flip between a dominant bacteriogenic or hydrothermal S source (Barrie et al., 2009). Fluid inclusion data from ore-stage minerals further reveals that the metal-bearing fluids were highly saline (10–25 wt% NaCl eq.) and relatively warm (150–250 °C) (Wilkinson and Hitzman, 2014; Yesaras et al., 2019). The cooler, bacteriogenic sulphur-rich fluids reveal medium-salinity, seawater-derived brines (Wilkinson et al., 2005). Recent clumped isotope work across the Irish Zn-Pb orefield, including Lisheen, further supports the dual fluid mixing model, revealing clear mixing trends between hydrothermal and brine fluid end-members (Hollis et al., 2024).

The LOM-hosted mineralisation exhibits a broadly similar S-isotope spectrum (Fig. 10a-b) to mineralisation elsewhere in the Irish Zn-Pb Orefield. The wide variability and overlap of $\delta^{34}S$ values, and textural associations, are consistent with the mixing model proposed for Waulsortian Limestone Formation-hosted orebodies both at Lisheen (Fig. 10c; Wilkinson et al., 2005; Doran et al, 2022) and elsewhere in Ireland (Boyce et al., 1983a; Anderson et al., 1998; Barrie et al., 2009). However, while many of the samples studied show variable $\delta^{34}S$ values corresponding to fluid mixing between hydrothermal and bacteriogenic S, an additional, minor source of S possibly exists in the LOM-hosted mineralisation that originates from the replacement of earlier formed sulphides at Lisheen. The role of replacement on S isotope values has been shown elsewhere at Lisheen, with the partial break-down of earlier formed pyrite thought to have facilitated remobilization and re-incorporation of S with low $\delta^{34}S$ values ($\ll$0 ‰) into later sphalerite and pyrite (Doran et al., 2022). Consequently, S from early pyrite may have been similarly liberated during later replacement (Figs. 4, 5) contributing to overlapping $\delta^{34}S$ values pyrite and sphalerite. It is predicted that replacive Sp2 incorporated Fe liberated during pyrite replacement, resulting in elevated Fe values relative to Sp1, which overgrows but does not replace pyrite. While no mineral chemical data is available from sphalerite in this study, Sp2 Fe analyses would provide a test of the replacement hypothesis. Moreover, the apparent lack of Py0 within the replacement-dominated steel ore is consistent with extensive replacement of pyrite and incorporation of Fe into replacive Sp2, and providing an additional S source for paragenetically later sulphides, though we cannot discount the possibility that Py0 was never present in the steel ore.

### *5.1.1. Pre- to early main ore stage*

Pre-ore hydrothermal activity in the LOM led to dissolution and dolomitisation of the host rock, and the formation of dolomite rims on newly formed open space (Fig. 4a). Dissolution and dolomitisation of the LOM took place in the footwall of major faults at Lisheen, leading to an increase in porosity and permeability of the host rocks (Hitzman et al., 2002). These processes were recorded as enabling brecciation of the LOM, primarily through solution collapse, resulting in breccias visually similar to black matrix breccias within the Waulsortian Limestone Formation as described by Hitzman et al. (2002) and Güven et al. (2023). The localisation of these processes adjacent to faults allowed later metal-bearing fluid movement into these breccias, which initiated with extensive pyrite formation, similar to conditions reported from the distal Island Pod orebody at Lisheen (Doran et al., 2022).

Early, hydrothermal ore stage pyrite can be classified broadly into two main forms based on textural and paragenetic relations. Each of

these pyrite phases display the influence of mixing between hydrothermal fluids and brines carrying bacteriogenically derived sulphur (e.g., metal zonation, S isotope values, and the presence of Cu, Tl, As; Figs. 4-5, 9). A clear progression towards more intensive hydrothermal (as opposed to bacteriogenic fluid) influence can be traced by the increasing S isotope ratios from Py0 to $Py1_{late}$ (Fig. 10a-b), indicating that the ramping up of the hydrothermal system was recorded in these pyrite phases.

The first pyrite (**Py0**) to form in the LOM mineralisation precipitated into open space left behind after the dissolution of the host and it replaced oolitic fragments and bioclastic material (Fig. 4b-c). This early pyrite has the lowest sulphur isotope compositions (−28.4 to −21.9 ‰) from all phases analysed, and S dominated by bacterially derived sulphide was the primary S source, with very limited hydrothermal S relative to later phases. However, Py0 has elevated Tl, Cu, Ni, and As consistent with the influence of hydrothermal fluids (Fig. 6). No equivalent phase to Py0 has been described elsewhere at Lisheen, with the first pyrite phase common to all parts of the Lisheen deposit being $Py1_{early}$. Paragenetically later pyrite grains exhibit zoned textures with trace element-rich (As, Cu, Ni, Tl) phases often associated with complex growth morphologies (initial $Py1_{early}$ and $Py1_{late}$), similar to textures observed elsewhere in Lisheen (Doran et al., 2022). The zoned morphologies of these pyrites are indicative of rapid precipitation from episodic pulses and fluid mixing, with each pulse representing changes in the mineralising fluid composition and/or temperature (Fleet et al., 1989; Shore and Fowler, 1996). The margins between successive zones of $Py1_{early}$ are sharp, suggesting no resorption, with each zone representing a fresh period of pyrite precipitation from hydrothermal fluid influx (Craig et al., 1998; Doran, 2021). Conversely, $Py1_{late}$ often has corroded margins with earlier phases, sometimes replacing $Py1_{early}$ and also contains the highest concentrations of As, Cu and Tl of all phases (Fig. 6). The elevated Cu associated with $Py1_{late}$ suggests its growth was related to hotter fluids than the previous pyrite phases (Fusciardi et al., 2003. Pyrite trace element systematics are sensitive to hydrothermal fluid temperature and composition changes, with element assemblages containing Co, Ni, Cu typically associated with > 300 °C fluids, while Pb, Ag and Tl are more often connected to 150–200 °C fluids (Steadman et al., 2021). The overlapping, but distinctive trace element assemblages of pyrite from the LOM indicate the early fluids were part of an evolving system with mixing of multiple hydrothermal pulses, and not separate events.

However, while $Py1_{early}$ has higher $\delta^{34}S$ values (−25.3 to −12.3 ‰) than Py0, the two phases display overlapping trace element concentrations, with Py0 generally hosting higher median concentrations of As, Ni, Tl, and Co possibly indicating preferential incorporation of As, Ni, Tl, and Co in co-precipitating phases (e.g., sulfosalts) while $Py1_{early}$ was crystallizing (Fig. 8). The variable development of trace element-rich phases across the Lisheen deposit also indicates that the reach of these fluids varied across the deposit, likely related to a dynamic complex, subseafloor fluid regime.

#### 5.1.2. Main ore stage mineralisation

Main ore stage mineralisation commenced with the formation of zoned (typically colloform), often red sphalerite. The subsequent change in colour from Sp1 to Sp2 to more medium/auburn brown may reflect a change in trace element concentration. The occurrence of colloform sphalerite suggests mixing between hydrothermal fluids and bacteriogenic brines was the main process responsible for early Zn mineralisation (Barrie et al., 2009; Gagnevin et al., 2014). This is also supported by sulphur isotopes in sphalerite. Sphalerite mineralisation generally has higher $\delta^{34}S$ values than earlier pyrite, with Sp2 generally containing higher $\delta^{34}S$ values (>0 ‰; Fig. 10) than Sp1. The higher $\delta^{34}S$ values of Sp2 indicate that more hydrothermal sulphur became available for incorporation during the main mineralisation as the hydrothermal system evolved. Moreover, after Sp1 mineralisation, repeated hydrothermal fluid events facilitated significant dissolution and reprecipitation of open space in the host rock. The extensive replacement of pyrite (Py0, $Py1_{early}$, $Py1_{late}$) by sphalerite from this stage (Sp2) led to botryoidal and irregular forms that crosscut zones in pyrite (e.g., Fig. 4f, k, and Fig. 5c-e, h). This texture is interpreted to be due to dissolution of pyrite and replacement by sphalerite due to mineral-hydrothermal fluid interaction (Finlow-Bates et al., 1977; Putnis and Ruiz-Agudo, 2013). The replacement of pyrite by Sp2 was most extensively developed in the steel ore region, indicating this area was subjected to more intensive hydrothermal activity than elsewhere in Lisheen. Successive mineralisation after sphalerite deposition is characterised by galena and tennantite (Fig. 4i-l), indicating that later hydrothermal pulses either introduced Pb into the system, or alternatively, caused a change in mineralising conditions (e.g., increased temperature, pH), favouring galena mineralising over sphalerite. Following this, Cu-mineralisation dominated, with chalcopyrite and bornite prevailing. This presence of copper minerals such as these has also been observed by Frenzel et al. (2024), who further suggested there may be more copper mineralisation at depth at deposits such as Lisheen.

There are additional processes that influence the geochemical signatures of phases in LOM-hosted mineralisation, despite having S isotope signatures influenced by fluid mixing, in line with those from previous studies at Lisheen (Fig. 10c). Although data are limited, the apparently lower $\delta^{34}S$ values of Gn1 (n = 4) and Gn2 (n = 4) relative to the paragenetically earlier Sp2 (n = 2) may be a result of new bacteriogenic sulphur influxes, or/and the replacement of $Py1_{early}$ and Sp1, where dissolution-replacement resulted in the release of sulphur into hydrothermal fluids, which was then re-incorporated into the later formed galena. The similarity in $\delta^{34}S$ values between Gn1 and Gn2, and earlier $Py1_{early}$ and Sp1 (Fig. 10), is strongly supportive of the latter process of sulphur recycling. This dissolution-replacement process has been shown not to fractionate sulphur isotopes significantly between source and fluid (Seal, 2006), and is therefore consistent with galena S isotope values (Fig. 10). However, the dominant ore $\delta^{34}S$ isotope values (~-4 to −18 ‰) at Lisheen (Wilkinson et al., 2005) suggest a consistent process is required across the deposit (i.e., fluid mixing), with replacement processes locally influencing S isotope values.

The steel ore region hosts extensive banded nickeline and gersdorffite prior to galena formation (Fig. 5c, g), at the same paragenetic stage as $Py1_{late}$ elsewhere in the LOM, possibly indicating localised fluid pulses with unique compositions that did not extend past the steel ore region. While tennantite is more abundant than tetrahedrite, localised veining by tetrahedrite suggests that a change in fluid conditions facilitated Sb and As precipitation from solution. These minerals were postdated by the subsequent formation of bornite and chalcopyrite (Fig. 4l), particularly extensive in the Main Zone compared to elsewhere at Lisheen, indicating that a resurgence of higher temperature (>300 °C), deeper-sourced, Cu-rich fluids influenced LOM-hosted mineralisation at this paragenetic stage (Fusciardi et al., 2003). The final fluid activity in the LOM led to the precipitation of dolomite, calcite and quartz (and possibly barite), with no significant Zn-Pb mineralisation associated with these phases, indicating a waning and cooling hydrothermal system (Wilkinson et al., 2005).

Several key processes are responsible for the variable sulphide mineralogy observed within LOM-hosted mineralisation, including sulphide replacement and fluid mixing. Initial hydrothermal activity initiated with episodic fluid flow and fluid mixing, as indicated by pyrite zonations. Later hydrothermal activity led to selective replacement of earlier sulphides, often more extensive in the Main Zone and the steel ore region, adjacent to known feeder faults. Further, replacement of earlier sulphides was facilitated by the presence of microfractures with subsequent replacement likely intensifying the microfracturing (Wagner and Cook, 1998), or alternatively fluids utilised grain boundaries leading to replacement. The presence of microfractures, enabling galena mineralisation, is particularly common in pyrite (Fig. 4f), likely due to its brittle nature. Furthermore, the enrichment of Cu, Ni, As and Sb in the LOM-hosted mineralisation, relative to other Waulsortian Limestone

Formation-hosted orebodies, is indicative of close proximity to 'feeder faults' where the hydrothermal fluids entered the system (Fusciardi et al., 2003; Torremans et al., 2018).

### 5.2. Metal distributions at Lisheen: Spatial and temporal variation trends, dissolution and replacement, fluid conduits and sources

Trace element analysis of sulphides from LOM-hosted mineralisation offers a unique opportunity to study early fluid activity, where hydrothermal fluids are thought to have first encountered a clean limestone at Lisheen (Güven et al., 2023). Variations related to distance from feeder faults are observable across Lisheen, with more typical hydrothermal elements (e.g., Cu, Ni) often concentrated in sulphides adjacent to fluid conduits. Sulphide morphologies also display more complex morphologies proximal to feeder zones, reflecting several dissolution and reprecipitation processes. Consequently, studies of LOM-hosted mineralisation can provide insights into the early hydrothermal processes and help us to decipher replacement textures as they relate to the larger ore system.

At Lisheen, whole-rock metal distribution patterns reveal that Waulsortian Limestone Formation-hosted Ag, Cd, Co, Cu and Ni concentrations are elevated proximal to hydrothermal feeder faults, becoming more depleted with increasing distance, resulting in zoned metal patterns (Fusciardi et al., 2003; Torremans et al., 2018). Similar zonation patterns are found in LOM-hosted mineralisation, with Ni, Co, As, Cu, Fe, Zn and Pb concentrations becoming progressively lower with increasing distance from faults interpreted to have acted as conduits for hydrothermal fluids (Fig. 3). The LOM also contains elevated levels of Ni and Cu phases relative to more distal Waulsortian Limestone Formation-hosted mineralisation, (Fig. 2; e.g., Doran et al., 2022). Nickel and Cu are typically associated with the presence of nickeline, gersdorffite, chalcopyrite and tennantite, which are not common in more distal parts of Lisheen (Doran et al., 2022). Within the distal Island Pod deposit, minor growth bands of nickeline and gersdorffite (Ni-rich) have been described from the same paragenetic stage as the LOM-hosted equivalents, but without chalcopyrite or tennantite (other Cu-rich phases) (Doran et al., 2021), likely indicating that in this deposit there was waning influence of hydrothermal fluids at the time of deposition or lower temperatures with increasing distance from feeder faults. This spatial variation is also noted from S isotope values from ore stage pyrite, with distal parts of Lisheen typically having lower S isotope values, reflecting an increased influence from bacteriogenic sulphur (e.g., Wilkinson et al., 2005; Doran et al., 2022).

While samples used in trace element studies were from a restricted number of boreholes/stockpile samples (ESM 1), they are considered representative of key textures and features across LOM-hosted regions based on observations from 100 + samples. LOM-hosted occurrences are less widespread than mineralisation within the Waulsortian Limestone Formation (Fig. 2a), but chemical trends between samples reveal variations associated with ore zones, suggesting hydrothermal fluid migration from the steel ore to Main Zone to Derryville Zone, with an additional hydrothermal pulse introducing new metals in the Ramp Zone (Fig. 7). The increase in metals in the Ramp Zone, and subsequent drop in the Derryville Zone (typically lower median values than the Main Zone; Fig. 7), suggests that an additional hydrothermal pulse entered the hydrothermal system via the relay ramp fault network near the Ramp Zone with a slightly different metal source, perhaps due to interaction with mafic or ultramafic rocks at depth. Such ore-scale variation has been detected by high precision Pb isotope analysis of galena from across the Rathdowney Trend, with variations between ore lenses thought to reflect variations in the underlying basement rocks and fluid pathways through the mineral system (Hollis et al., 2019), and thus appears to be a common feature to the Irish Orefield.

Pyrite data from the Island Pod orebody suggest an approximately northward migration of fluids, with early Py (equivalent to LOM $Py1_{early}$) having lower concentration of many hydrothermal elements (e.g., Ni, Co, Tl, As, Cu) relative to LOM-hosted mineralisation (Doran et al., 2022). This study also revealed variation on a smaller scale, with concentrations of Tl and As in pyrite decreasing by 40–80 % from samples within the orebody compared to those in the surrounding sub-economic halo (Doran et al., 2022). Pyrite from the Island Pod orebody ($Py1_{early}$ equivalent) also exhibited elevated Ni (up to ~ 11 wt%) and Co in early bands, with later coarse forms of $Py1_{early}$ typically depleted relative to the LOM (Doran et al., 2022). Cobalt in these later forms was often below detection levels (<0.01 wt%) with Ni remaining elevated relative to the LOM $Py1_{early}$ (Doran et al., 2022). In general, Ni is less abundant in the Island Pod, with other Ni-bearing phases (e.g., niccolite) that are recorded in the more proximal steel ore region being absent from the Island Pod. Like other transition metals, Ni may be mobilised under Cl-bearing hydrothermal fluid conditions (En-Naciri et al., 1997; Brugger et al., 2016), such as those found at Lisheen (Wilkinson et al., 2005), likely explaining its presence in the distal Island Pod orebody.

The abundance of Ni-bearing sulfosalts (e.g., Fig. 5) in LOM-hosted mineralisation has previously been suggested to reflect the early interaction of hot, hydrothermal fluids, where Ni dropped out of solution when it left the feeder pathway (Passmore, 2002). The $\delta^{34}S$ values presented here confirm the fluids that led to early Fe- and subsequent Ni-rich mineral precipitation in the LOM were dominantly hydrothermal in origin. Additionally, the appearance of Ni minerals (e.g. gersdorffite and nickeline) after the bulk of early Fe mineralisation (forming bands around earlier pyrite) suggests an increase in Ni-bearing fluids and/or a decrease in available sulphur, as both minerals contain significant arsenide. Whereas early pyrite forms do contain Ni, there was likely not sufficient concentration to form Ni minerals like gersdorffite and nickeline. This suggests that the fluids that led to early pyrite and Ni mineral precipitation were related, further indicating a hydrothermal over diagenetic (e.g. seawater) source for Ni within the LOM. The greater occurrence of Ni minerals in the steel ore region relative to the rest of the LOM-hosted mineralisation further suggests that Ni preferentially precipitated out of solution early, at interpreted feeder fault intersections.

Within the steel ore, As appears to have a different relationship with pyrite than elsewhere at Lisheen (Fig. 6b, c). This change in As behaviour may indicate the preferential incorporation of As into other phases (e.g. arsenopyrite) outside of the steel ore or be due to another As source affecting this area. Nickeline and gersdorffite are commonly observed in the steel ore region along with pyrite, with the extensive replacement textures suggesting it was subjected to more variable and intensive hydrothermal activity than elsewhere at Lisheen, causing more complex trace element assemblages, as shown by the studied pyrite. Further, the variable As concentrations in steel ore hosted pyrite compared to elsewhere in the LOM, may indicate hydrothermal pulses impacted the steel ore that did not migrate through the other zones.

Pyrite **Co/Ni ratios** have widely been considered important in ore genesis and characterization, along with fluid source discrimination (Loftus-Hills and Soloman, 1967; Bralia et al., 1979; Reich et al., 2016; del Real et al., 2020). In general, Co/Ni ratios < 1 are generally thought to indicate a sedimentary pyrite origin, with Ni sourced from seawater. The Co/Ni ratios of pyrite from this study are highly variable, with ratios both < 1 and > 1 further suggesting multiple sources, in agreement with our S isotope data. However, the application of this method has limitations, with ratio interpretations very dependent on knowing the environment of formation. Nickel is typically concentrated in magmatic sulphide and weathered laterite deposits (Fan and Gerson, 2011), and its hydrothermal enrichment has been related to ultramafic/mafic source rocks in several deposits globally (e.g., Avebury nickel deposit, Tasmania, González-Álvarez et al., 2010; Keays and Jowitt, 2013; Enterprise nickel deposit, Zambia, Capistrant et al., 2015; Nimbus hybrid VMS-epithermal deposit, Australia, Hollis et al., 2021). Consequently, there may be unknown mafic/ultramafic bodies preserved at depth underlying the Rathdowney Trend within Palaeozoic basement rocks, which corresponds to Pb isotope data from Lisheen (Hollis et al., 2019; in

prep.). A similar relationship has been seen elsewhere in Ireland, such as the Cummer serpentine belt which is found along strike in the Wicklow fault zone, southeast Ireland (e.g., Gallagher, 1989).

The sources of Cu in the Irish Orefield are still widely debated, with the Old Red Sandstone (ORS) thought to be a trap (not a source) for Cu in the southern Irish Orefield (Everett et al., 2003; Wilkinson, 2023). The transport of Cu in the Irish Orefield appears to be closely dependant on the availability of fluid pathways (i.e., faults) that allow movement through the underlying ORS, while also requiring specific temperature +/- salinity fluid conditions (Wilkinson, 2023).

## 6. Conclusions

Lisduff Oolite Member (LOM)-hosted sulphides display unique characteristics and mineral assemblages. Within LOM-hosted mineralisation, several generations of Fe-, Zn-, Pb-, Cu- and Ni-minerals are identified, with complex textural and chemical associations due to its location proximal to feeder faults and consequent more intense hydrothermal activity. The LOM records an important part of the ascending hydrothermal pathway that ultimately resulted in the bulk of mineralisation in the Waulsortian Limestone Formation. This study presents new insights into the paragenesis, mineral chemistry, and sulphur isotope characteristics of LOM-hosted Zn-Pb-Cu-Ni mineralisation at Lisheen, providing a refined understanding of sulphide formation, fluid mixing, and metal sources in Irish-type systems. The ore textures and metal distribution patterns presented here build upon existing deposit-scale frameworks that discuss LOM-hosted mineralisation at Lisheen.

- Multistage sulphide paragenesis and sulphur isotope characteristics: The first generation of pyrite (Py0; $\delta^{34}S$ = –28.4 to –21.9 ‰) in the LOM has not been described elsewhere at Lisheen. This is followed by Py1 ($\delta^{34}S$ = –25.3 to –7.4 ‰) which is the first consistent pyrite phase between differing hosts, and reveals more characteric fluid mixing S isotopes values. $Py1_{late}$ hosts the highest concentrations of As (up to 6.9 wt%), Cu (up to 0.53 wt%), Ni (up to 1.02 wt%) and Tl (up to 0.39 wt%) of all pyrite phases, recording an increased influence of hydrothermal with paragenetic stage.
- Initial Py0, including early trace element enriched forms of $Py1_{early}$, were not observed in the steel ore region, possibly due to extensive replacement or preferential incorporation of elements into sulfosalts.
- The similar morphologies and trace element trends for early pyrite ($Py1_{early}$) between the distal Island Pod and LOM-hosted orebodies suggest that similar hydrothermal processes led to their formation. However, the generally lower trace element values of $Py1_{early}$ between orebodies may indicate the overall northward migration of fluids.
- Sulphur isotope data support a dual fluid mixing model of formation, similar to WLF-hosted mineralisation. The isotopic spectrum spans a wide range ($\delta^{34}S$ = –28.4 to + 1.6 ‰), consistent with dual-source mixing. Notably, the lowest values are in early pyrite (Py0), while later sphalerite and galena are defined by heavier isotopic values (Sp2: up to + 1.6 ‰; Gn1: –14.0 to –4.7 ‰), indicating increasing hydrothermal input and potential sulphur recycling during replacement.
- Nickeline and gersdorffite are commonly observed in the steel ore region with pyrite, indicating a distinct high-temperature, Ni-rich environment, which was subjected to increased hydrothermal fluid pulses compared to other regions at Lisheen. These phases are not observed in more distal zones, suggesting localisation near feeder faults. Galena and tennantite mineralisation followed this phase, marking a shift in metal availability and fluid chemistry.

These results establish the LOM as a key recorder of early fluid–rock interactions at Lisheen, and record valuable information about early ore forming and hydrothermal processes at Lisheen. This demonstrates that $\delta^{34}S$ and pyrite mineral chemistry, S isotope analysis, and petrographic studies are effective tools for identifying hydrothermal fluid pathways in carbonate-hosted Zn-Pb systems. These results have implications for targeting similar carbonate-hosted systems globally, especially where deeper or structurally complex ore zones remain underexplored.

## Declaration of competing interest

The authors declare the following financial interests/personal relationships which may be considered as potential competing interests: Aileen L. Doran reports financial support was provided by Ireland Canada University Foundation. If there are other authors, they declare that they have no known competing financial interests or personal relationships that could have appeared to influence the work reported in this paper.

## Acknowledgements

The authors thank the editor and all reviewers for their feedback and suggestions. Vedanta Resources are thanked for access to the Lisheen mine and drill core. Microscopy and SEM images were acquired at University College Dublin (UCD). Sulphur isotope analysis was carried out at Scottish Universities Environmental Research Centre (SUERC), with support from technician Alison McDonald. Cathodoluminescence analysis was completed at Imperial College London, with direction from Jonathan Watson. EMPA analyses were conducted at Memorial University Newfoundland (MUN) with guidance from Wanda Aylward. Additionally, the authors wish to thank the UCD-iCRAG Raw Materials group for discussions around the presented data and help in sample collection, including but not limited to Dr Roisin Kyne, Dr John Conneally, Rob Doyle, Dr Sean Johnson, Dr Oakley Turner.

This publication has emanated from research conducted with the financial support of Science Foundation Ireland (SFI) (now Research Ireland) under Grant Number 13/RC/2092 and co-funded under the European Regional Development Fund. Part of this research has been made possible by a James M Flaherty Research Scholarship from the Ireland Canada University Foundation, with the assistance of the Irish Government. Additional research was facilitated by the Steven M. Millan Scholarship.

## Appendix A. Supplementary data

Supplementary data to this article can be found online at https://doi.org/10.1016/j.oregeorev.2025.106660.

## Data availability

Data used in this research is available in ESM 1, associated with this article and they can also be obtained from the author through.

## References

AECOM, 2020. A social, environmental and economic assessment of Galmoy and Lisheen Mines. Report to the Department of Communications, Climate Action and Environment. 209p. Accessed online (02/06/2023): https://www.gov.ie/en/publication/29332-a-social-environmental-and-economic-assessment-of-galmoy-and-lisheen-mines/.

Anderson, I.K., Ashton, J.H., Boyce, A.J., Fallick, A.E., Russell, M.J., 1998. Ore depositional processes in the Navan Zn-Pb deposit, Ireland. Econ. Geol., 93, 535–563.

Andrew, C.J., 1986. A diagrammatic representation of the Courceyan stratigraphy of the Irish Midlands. In: Andrew, C.J., Crowe, R.W.A., Finlay, S., Pyne, J.F. (Eds.), Geology and Genesis of Mineral Deposits in Ireland. Irish Assoc. for Econ. Geol, Dublin, pp. 239–241.

Andrew, C.J., 2023, The Sedmochislenitsi Zn-Pb-Cu-Ag deposit, NW Bulgaria: could it be Irish-type? A review of the evidence. In: Andrew, C.J., Hitzman, M.W., and Stanley, G. 'Irish-type Deposits around the world': Irish Assoc. for Econ. Geol., p. 407-424. DOI: https://doi.org/10.61153/MOXI6363.

Ashton, J.H., Andrew, C.J., and Hitzman, M.W., 2023, Irish-type Zn-Pb deposits - What are they and can we find more?, In: Andrew, C.J., Hitzman, M.W., and Stanley, G.

'Irish-type Deposits around the world': Irish Assoc. for Econ. Geol., p. 95-146. DOI: https://doi.org/10.61153/DODR7609Dunlevy,.
Banks, D.A., Boyce, A.J., Samson, I.M., 2002. Constraints on the origins of fluids forming Irish Zn-Pb-Ba deposits: Evidence from the composition of fluid inclusions. Econ. Geol., 97 (3), 471–480.
Barrie, C.D., Boyce, A.J., Boyle, A.P., Williams, P.J., Blake, K., Wilkinson, J.J., Lowther, M., McDermott, P., Prior, D., 2009. On the growth of colloform textures: a case study of sphalerite from the Galmoy ore body, Ireland. J. Geol. Soc London 166, 563–582.
Blakeman, R.J., Ashton, J.H., Boyce, A.J., Fallick, A.E., Russell, M.J., 2002. Timing of Interplay between Hydrothermal and Surface Fluids in the Navan Zn + Pb Orebody, Ireland: Evidence from Metal Distribution Trends, Mineral Textures, and $\delta^{34}S$ Analyses. Econ. Geol., 97, 73–91.
Boyce, A.J., Anderton, R., Russell, M.J., 1983a. Rapid subsidence and early Carboniferous base-metal mineralization in Ireland. Trans. Instn. Min. Metall. (sect b: Appl. Earth Sci.), 92, 55–66.
Boyce, A.J., Coleman, M.L., Russell, M.J., 1983b. Formation of fossil hydrothermal chimneys and mounds from Silvermines, Ireland. Nat., 306, 545–550.
Bralia, A., Sabatini, G., Troja, F., 1979. A revaluation of the Co/Ni ratio in pyrite as geochemical tool in ore genesis problems: Min. Depos., 14, 353–374.
Brugger, J., Liu, W., Etschmann, B., Mei, Y., Sherman, D.M., Testemale, D., 2016. A review of the coordination chemistry of hydrothermal systems, or do coordination changes make ore deposits? Chem. Geol., 447, 219–253.
Capistrant, P.L., Hitzman, M.W., Kelly, N., Wood, D., Kui-per, Y., Jack, D., Stein, H., 2015. Geology of the Enterprise hydrothermal nickel deposit, North-western Province, Zambia. Econ. Geol., 110, 9–38.
Cordeiro, P., dos Santos, A.M., Steed, G., de Araújo Silva, A., Meere, P., Corcoran, L., Simonetti, A., Unitt, R., 2023. The carbonate-hosted Gortdrum Cu-Ag(±Sb-Hg) deposit, SW Ireland: C-O-Sr-Nd isotopes and whole-rock geochemical signatures. J. Geochem. Explo., 248. https://doi.org/10.1016/j.gexplo.2023.107196.
Craig, J.R., Vokes, F.M., Solberg, T.N., 1998. Pyrite: physical and chemical textures. Min. Dep., 34, 82–101.
del Real, I., Thompson, J.F.H., Simon, A.C., Reich, M., 2020. Geochemical and Isotopic Signature of Pyrite as a Proxy for Fluid Source and Evolution in the Candelaria-Punta del Cobre Iron Oxide Copper-Gold District, Chile. Econ. Geol., 115 (7), 1493–1518.
Doran, A.L., 2021. Geochemical investigations of mineralising processes in the southern Irish Zn-Pb orefield: the combined application of isotope (S, clumped O-C, Sr, H) and mineral chemistry studies to track fluid flow: Unpublished. University College Dublin, Dublin, School of Geosciences. Ph.D. thesis.
Doran, A.L., Hollis, S.P., Menuge, J.F., Piercey, S.J., Boyce, A.J., Güven, J., Turner, O., 2022. A distal, high-grade Irish-type orebody: petrographic, sulfur isotope, and sulfide chemistry of the Island Pod Zn-Pb orebody, Lisheen, Ireland. Econ. Geol., 117 (2), 305–326.
Doyle, R., 2022. Regional variations of Tournaisian and Viséan lithostratigraphy and their links to basin and structural evolution in Ireland. Research Masters Thesis. University College Dublin.
Dunlevy, E., Torremans, K., Holdstock, M., and Hitzman, M., 2023, A new look at the Gortdrum copper deposit, Co. Tipperary, Ireland. In: Andrew, C.J., Hitzman, M.W., and Stanley, G. 'Irish-type Deposits around the world': Irish Assoc. for Econ. Geol., p. 363-370. DOI: https://doi.org/10.61153/JLTX1259.
Earls, G., 1994, The Lisheen Zn-Pb deposit: Mining Mag., v. July, p. 6-8.
En-Naciri, A., Barbanson, L., Touray, J.-C., 1997. Brine inclusions from the Co-As(Au) Bou Azzer District, Anti-Atlas Mountains, Morocco. Econ. Geol., 92 (3), 360–367.
Everett, C.D., Rye, D.M., Wilkinson, J.J., Boyce, A.J., Ellam, R.M., and Fallick, A.E., 1999, The genesis of Irish-type Zn-Pb deposits: Characterisation and origin of the principal ore fluid, in Stanley, C.J., eds., Mineral Deposits: Process. to Process., v. 1 and 2. A.A.: Rotterdam, Balkema Publishers, p. 845-848.
Everett, C.E., Rye, D.M., Ellam, R.M., 2003. Source or sink? An assessment of the role of the Old Red Sandstone in the genesis of the Irish Zn-Pb Deposits. Econ. Geol., 98, 31–50.
Eyre, S.L., 1998, Geochemistry of dolomitization and Zn-Pb mineralization in the Rathdowney Trend, Ireland: Unpublished Ph.D. thesis, London, Royal School of Mines, Imperial College of Science Technology and Medicine.
Fallick, A.E., Ashton, J.H., Boyce, A.J., Ellam, R.M., Russell, M.J., 2001. Bacteria were responsible for the magnitude of the world-class hydrothermal base metal sulfide orebody at Navan, Ireland. Econ. Geol., 96, 885–890.
Fan, R., Gerson, A.R., 2011. Nickel geochemistry of a Philippine laterite examined by bulk and microprobe synchrotron analyses. Geochim. Et Cosmochim. Acta 75 (21), 6400–6415.
Finlow-Bates, T., Croxford, N.J.W., Allan, J.M., 1977. Evidence for, and implications of, a primary FeS phase in the lead-zinc bearing sediments at Mount Isa. Mineral Dep., 12, 143–149.
Fleet, M.E., MacLean, P.J., and Barbier, J., 1989, Oscillatory-Zoned As-Bearing Pyrite from Strata-Bound and Stratiform Gold Deposits: An Indicator of Ore Fluid Evolution, in Keays, R.R., Ramsay, W.R.H., Groves, D.I., eds., The Geology of Gold Deposits: The Perspective in 1988: The Econ. Geol. Publishing Company, p. 356-362.
Frenzel, M., Röhner, M., Cook, N.J., Gilbert, S., Ciobanu, C.L., Güven, J.F., 2024. Mineralogy, mineral chemistry, and genesis of Cu-Ni-As-rich ores at Lisheen, Ireland. Min. Dep. https://doi.org/10.1007/s00126-024-01299-8.
Fusciardi, L.P., Güven, J.F., Stewart, D.R.A., Carboni, V., and Walsh, J.J., 2003, The geology and genesis of the Lisheen Zn-Pb deposit, Co. Tipperary, Ireland, in Kelly, J. G., Andrew, C.J., Ashton, J.H., Boland, M.B., Earls, G., Fusciardi, L., and Stanley, G., eds., Europe's Major Base Metal Deposits: Dublin, Irish Assoc. for Econ. Geol., p. 455-476.
Gagnevin, D., Menuge, J.F., Kronz, A., Barrie, C., Boyce, A.J., 2014. Minor elements in layered sphalerite as a record of fluid origin, mixing, and crystallization in the Navan Zn-Pb ore deposit, Ireland. Econ. Geol., 109, 1513–1528.
Gallagher, V., 1989. The occurrence, textures, mineralogy and chemistry of a chromite-bearing serpentinite, Cummer, Co. Wexford: Geol. Survey Ireland Bull. 4, 89–98.
Geological Survey Ireland, 2014, Bedrock geology of Ireland map 1:50,000: Geol. Survey Ireland, Dublin.
González-Álvarez, I., Porwal, A., Beresford, S.W., McCuaig, T.C., Maier, W.D., 2010. Hydrothermal Ni prospectivity analysis of Tasmania, Australia. Ore Geol. Rev., 38 (3), 168–183.
Güven, J., Torremans, K., Johnson, J., Hitzman, M., 2023, The Rathdowney Trend, Ireland: Geological evolution and controls on Zn-Pb mineralization. In: Andrew, C., Hitzman, M., Stanley, G., 50 years of Irish-type Zn-Pb deposits.
Hitzman, M.W., 1993, Sulfur isotope data from the Lisheen mine: internal company report.
Hitzman, M.W., Large, D., 1986. A review and classification of the Irish carbonate-hosted base metal deposits. In: Andrew, C.J., Crowe, R.W.A., Finlay, S., Pyne, J.F. (Eds.), Geology and Genesis of Mineral Deposits in Ireland. Irish Assoc. for Econ. Geol, Dublin, pp. 217–238.
Hitzman, M.W., O'Connor, P.G., Shearley, E., Schaffalitzky, C., Beatty, D.W., Allan, J.R., and Thompson, T., 1992, Discovery and geology of the Lisheen Zn-Pb-Ag prospect, Rathdowney trend, Ireland, in Bowden, A.A., Earls, G., O'Connor, P.G., and Pyne, J. F., eds., The Irish Minerals Industry 1980-1990: Dublin, Irish Assoc. for Econ. Geol., p. 227-246.
Hitzman, M.W., Allan, J.R., Beaty, D.W., 1998. Regional dolomitization of the Waulsortian limestone in southeastern Ireland: Evidence of large-scale fluid flow driven by the Hercynian orogeny. Geol., 26, 547–550.
Hitzman, M.W., 1999. Extensional faults that localize Irish syndiagenetic Zn-Pb deposits and their reactivation during Variscan compression. Geol. Soc., London, Special Publications 155 (1), 233–245.
Hitzman, M.W., Redmond, P.B., Beaty, D.W., 2002. The carbonate-hosted Zn-Pb-Ag deposit, County Tipperary, Ireland. Econ. Geol., 97, 1627–1655.
Hollis, S.P., Doran, A.L., Menuge, J.F., Daly, J.S., Guven, J., Piercey, S.J., Cooper, M., Turner O. & Unitt, R., 2019, Mapping Pb isotope variations across Ireland: from terrane delineation to deposit-scale fluid flow: SGA 2019, Glasgow, 27th-30th August. [Oral Presentation by SPH].
Hollis, S.P., Dennis, P.F., Menuge, J.F., Doran, A.L., Marca, A., Davidheiser-Kroll, B., Wilkinson, J.J., Snell, K.E., Turner, O., Güven, J., Boyce, A., 2024. Tracking fluid temperature and δ18o in carbonate-hosted hydrothermal ore systems using clumped c-o isotopes. Econ. Geol., 119 (6), 1369–1382.
Hollis, S.P., Foury, S., Caruso, S., Johnson, S., Barrote, V., Pumphrey, A., 2021. Lithogeochemical and hyperspectral halos to Ag-Zn-(Au) mineralization at Nimbus, Eastern Goldfields Superterrane, Western Australia. Min., 11, 254.
Hnatyshin, D., Creaser, R.A., Wilkinson, J.J., Gleeson, S.A., 2015. Re-Os dating of pyrite con-firms an early diagenetic onset and extended duration of mineralization in the Irish Zn-Pb ore field. Geol., 43, 143–146.
Johnston, J.D., 1999. Regional fluid flow and the genesis of Irish Carboniferous base metal deposits. Min. Dep., 34, 571–598.
Johnston J. D., Coller, D., Millar, G., and Critchley, M. F., 1996, Basement structural controls on Carboniferous-hosted base metal mineral deposits in Ireland, in Strongen, P., Somerville, I. D., and Jones, G. LL., eds., Recent Advances in Lower Carboniferous Geology: Geol. Soc. Special Publication No. 107, pp. 1-21.
Keays, R.R., Jowitt, S.M., 2013. The Avebury Ni deposit, Tasmania: a case study of an unconventional nickel deposit. Ore Geol. Rev. 52, 4–17.
Kyne, R., Torremans, K., Güven, J., Doyle, R., Walsh, J., 2019. Structural controls on the formation of Irish Zn-Pb deposits: A case study on the Lisheen and Silvermines deposits, Co. Tipperary, Ireland. Econ. Geol., 114, 93–116.
Lee, M.J., Wilkinson, J.J., 2002. Cementation, hydrothermal alteration, and Zn-Pb mineralization of carbonate breccias in the Irish Midlands: Textural evidence from Cooleen Zone, near Silvermines, County Tipperary. Econ. Geol., 97, 653–662.
Loftus-Hills, G., Soloman, M., 1967. Cobalt, nickel and selenium in sulphides as indicators of ore genesis. Min. Dep. 2, 228–242.
Lyons, C., 2019, Petrographic and Isotopic Analysis of the Lisduff Oolite Member, Lisheen, Co. Tipperary, Ireland: Unpublished Undergraduate project report. Dublin, Earth Science Department, University College Dublin.
Paradis, S., 2007, Isotope geochemistry of the Prairie Creek carbonate-hosted zinc-lead-silver deposit, southern Mackenzie Mountains, Northwest Territories, in Mineral and Energy Resource Potential of the Proposed Expansion to the Nahanni National Park Reserve, North Cordillera, Northwest Territories, (ed.) H. Falck, D.F. Wrigh, and J. Harrist; Geological Survey of Canada, Open File, p. 5344.
Passmore, M., 2002, Main South Nickel Study: internal Vedanta company Lisheen mine report.
Philcox, M.E., 1984. Lower Carboniferous lithostratigraphy of the Irish Midlands: Dublin, Irish Assoc. for. Econ. Geol., 89.
Philcox, M.E., 2004. Nature and Origin of the Oolite Breccia. Internal report for Vedanta Resources, Lisheen Mine, p. 86.
Philips, W.E., Sevastopulo, G.D., 1986. The stratigraphic and structural setting of Irish mineral deposits. In: Andrew, C.J., Crowe, R.W.A., Finlay, S., Pyne, J.F. (Eds.), Geology and Genesis of Mineral Deposits in Ireland. Irish Assoc. for Econ. Geol, Dublin, pp. 1–30.
Putnis, C.V., Ruiz-Agudo, E., 2013. The mineral-water interface: where minerals react with the environment. Elem., 9, 177e182.
Qiu, W.J., Zhou, M.-F., Williams- Jones, A.E., 2024. Numerical simulation of the self-organizational origin of concentrically zoned aggregates of siderite and pyrite in sediment-hosted massive sulfide deposits. J. Geophys. Res.: Solid Earth 129, e2023JB028101. https://doi.org/10.1029/2023JB028101.

Rajabi, A., Mahmoodi, P., Rastad, E., Canet, C., Alfonso, P., Niroomand, S., Tarmohammadi, A., Perrnajmodin, H., and Akbari, Z., 2023, An introduction to Irish-type Zn-Pb deposits in early Cretaceous carbonate rocks of Iran, In: Andrew, C. J., Hitzman, M.W., and Stanley, G. 'Irish-type Deposits around the world', Irish Assoc. for Econ. Geol., p. 511-532. DOI: https://doi.org/10.61153/ZZUG6529.

Redmond, P.B., 1997, Structurally controlled mineralization and hydrothermal dolomitization at the Lisheen Zn-Pb-Ag deposit, Co. Tipperary, Ireland: Unpublished M.Sc. thesis, Trinity College Dublin.

Reich, M., Simon, A., Deditius, A., Barra, F., Chryssoulis, S., Lagas, G., Tardani, D., Knipping, J., Bilenker, L., Sánchez-Alfaro, P., Roberts, M.P., Munizaga, R., 2016. Trace element signature of pyrite from the Los Colorados iron oxide-apatite (IOA) deposit, Chile: A missing link between Andean IOA and iron oxide copper-gold systems? Econ. Geol., 11, 743–761.

Robinson, B.W., Kusakabe, M., 1975. Quantitative preparation of sulfur dioxide for 34S/32S analyses, from sulfides by combustion with cuprous oxide. Anal. Chem., 47, 1179–1181.

Röhner, M., 2017, Detailed characterisation of Cu-Co-Ni-As mineralisation at Lisheen Zn-Pb deposit, County Tipperary, Ireland: Unpublished master's thesis, Germany, TU Bergakademie Freiberg, Institute of Mineralogy, Department of Econ. Geol.

Savard, M.M., Chi, G., 1998. Cation Study of Fluid Inclusion Decrepitates in the Jubilee and Gays River (Canada) Zn-Pb Deposits - Characterization of Ore-Forming Brines. Econ. Geol., 93, 920–931.

Seal II, R.R., 2006. Sulfur isotope geochemistry of sulfide minerals. Rev. Min. Geochem., 61, 633–677.

Sevastopulo, G.D., and Redmond, P., 1999, Age of mineralization of carbonate-hosted, base metal deposits in the Rathdowney Trend, Ireland, in McCaffrey, K.J.W., Lonergan, L., and Wilkinson, J.J., eds., Fractures, Fluid Flow and Mineralization: London, Geol. Soc. Special Publications, v. 151, p. 303-311.

Shearley, E., Hitzman, M.W., Walton, G., Redmond, P., Davis, R., King, M., Duffy, L., and Goodman, R., 1992, Structural controls of mineralization, Lisheen Zn-Pb-Ag deposit, Co. Tipperary, Ireland: Geol. Soc. of America Abstracts with Program, v. 24, p. A354.

Shearley, E., Redmond, P., King, M., and Goodman, R., 1996, Geological controls on mineralization and dolomitization of the Lisheen Zn-Pb-Ag deposit, Co. Tipperary, Ireland, in Strogen, P., Somerville, I.D., and Jones, G.L., eds., Recent Adv. in Lower Carb. Geol.: London, Geol. Soc. Special Publication, v. 207, p. 23-33.

Shore, M., Fowler, A.D., 1996. Oscillatory zoning in minerals: a common phenomenon. The Canadian Min., 34, 1111–1126.

Slezak, P., Hitzman, M.W., van Acken, D., Dunlevy, E., Chew, D., Drakou, F., Holdstock, M., 2022 Petrogenesis of the Limerick Igneous Suite: insights into the causes of post-eruptive alteration and the magmatic sources underlying the Iapetus Suture in SW Ireland, p. 1-22.

Steadman, J.A., Large, R.R., Olin, P.H., Danyushevsky, L.V., Meffre, S., Huston, D., Fabris, A., Lisitsin, A., Wells, T., 2021. Pyrite trace element behavior in magmatichydrothermal environments: An LA-ICPMS imaging study. Ore. Geol. Rev. 128, 103878.

Torremans, K., Kyne, R., Doyle, R., Güven, J., Walsh, J.J., 2018. Controls on metal distribution at the Lisheen and Silvermines deposits: insights into fluid flow pathways in Irish-type Zn-Pb deposits. Econ. Geol., 113, 1455–1477.

Turner, O., 2019. Geochemical vectoring for Irish-type Zn-Pb deposits along the Rathdowney trend, Ireland: Unpublished. Dublin, Department of Geology, Trinity College Dublin. Ph.D. thesis.

Velasco, F., Herrero, J.,M., Yusta, I., Alonso, J.A., Seebold, I., Leach, D., 2003, Geology and Geochemistry of the Reocín Zinc-Lead Deposit, Basque-Cantabrian Basin, Northern Spain, Econ. Geol., v. 98 (7), p. 1371–1396. doi: https://doi.org/10.2113/gsecongeo.98.7.1371.

Wagner, T., Cook, N.J., 1998. Sphalerite remobilization during multistage hydrothermal mineralization events – examples from siderite-Pb-Zn-Cu-Sb veins, Rheinisches Schiefergebirge, Germany. Min. Petrol., 63, 223–241.

Wagner, T., Boyce, A.J., Fallick, A.E., 2002. Laser combustion analysis of $\delta^{34}S$ of sulfosalt minerals: Determination of the fractionation systematics and some crystal-chemical considerations. Geochim. et Cosmoch Acta 66, 2855–2863.

Walshaw, R.D., Menuge, J.F., Tyrrell, S., 2006. Metal sources of the Navan carbonate-hosted base metal deposit, Ireland: Nd and Sr isotope evidence for deep hydrothermal convection. Min. Dep., 41, 803–819.

Wilkinson, J.J., 2003. On diagenesis, dolomitization and mineralisation in the Irish Zn-Pb orefield: Min. Dep., 38, 968–983.

Wilkinson, J.J., 2010. A review of fluid inclusion constraints on mineralization in the Irish ore field and implications for the genesis of sediment-hosted Zn-Pb deposits. Econ. Geol., 105, 417–442.

Wilkinson, J.J., 2014, Sediment-Hosted Zinc-Lead Mineralization, in Holland, H.D., and Turekian, K.K., eds., Treat. on Geochem., 2nd ed.: Oxford, Elsevier, p. 219-249.

Wilkinson, J.J., Eyre, S.L., Boyce, A.J., 2005. Ore-forming processes in Irish-type carbonate-hosted Zn-Pb deposits: evidence from mineralogy, chemistry, and isotopic composition of sulfides at the Lisheen mine. Econ. Geol., 100, 63–86.

Wilkinson, J.J., Stoffell, B., Wilkinson, C.C., Jeffries, T.E., Appold, M.S., 2009. Anomalously metal-rich fluids form hydrothermal ore deposits. Science 323 (5915), 764–767.

Wilkinson, J.J., Crowther, H.L., Coles, B.J., 2011. Chemical mass transfer during hydrothermal alteration of carbonates: Controls of seafloor subsidence, sedimentation and Zn-Pb mineralization in the Irish Carboniferous. Chem. Geol., 289, 55–75.

Wilkinson, J.J., 2023, Tracing metals from source to sink in Irish-type Zn-Pb(-BaAg) deposits, In: Andrew, C.J., Hitzman, M.W., and Stanley, G. 'Irish-type Deposits around the world': Irish Assoc. for Econ. Geol., p. 147-168. DOI: https://doi.org/10.61153/QAIF6416.

Wilkinson, J.J., and Hitzman, M., 2014, The Irish Zn-Pb orefield: The view from 2014, in Archibald, S.M., and Piercey, S.J., eds., Current perspectives on zinc deposits: Dublin, Ireland, Irish Assoc. for Econ. Geol., p. 59–72.

Yesares, L., Drummond, D., Hollis, S.P., Doran, A.L., Menuge, J.F., Boyce, A.J., Blakeman, R., Ashton, R., 2019. Coupling mineralogy, textures, stable and radiogenic isotopes in identifying ore-forming processes and vectoring possibilities in Irish-type carbonate hosted Zn-Pb deposits. Min., 9 (335), 1–27.